Molecular Microbiology (2016) 99(6), 1099–1118 ■
doi: 10.1111/mmi.13292
First published online 10 February 2016

A phospholipase A_1 antibacterial Type VI secretion effector interacts directly with the C-terminal domain of the VgrG spike protein for delivery

Nicolas Flaugnatti,[1] Thi Thu Hang Le,[2,3] Stéphane Canaan,[4] Marie-Stéphanie Aschtgen,[1†] Van Son Nguyen,[2,3] Stéphanie Blangy,[2,3] Christine Kellenberger,[2,3] Alain Roussel,[2,3] Christian Cambillau,[2,3] Eric Cascales[1] and Laure Journet[1]*

[1]*Laboratoire d'Ingénierie des Systèmes Macromoléculaires, CNRS – Aix-Marseille Université, UMR 7255, Institut de Microbiologie de la Méditerranée, 31 Chemin Joseph Aiguier, 13402 Marseille Cedex 20, France.*
[2]*Architecture et Fonction des Macromolécules Biologiques, CNRS – UMR 7257, Campus de Luminy, Case 932, 13288 Marseille Cedex 09, France.*
[3]*Architecture et Fonction des Macromolécules Biologiques, Aix-Marseille Université, Campus de Luminy, Case 932, 13288 Marseille Cedex 09, France.*
[4]*Laboratoire d'Enzymologie Interfaciale et de Physiologie de la Lipolyse, CNRS – Aix-Marseille Université, UMR 7282, 31 Chemin Joseph Aiguier, 13402 Marseille Cedex 20, France.*

Summary

The Type VI secretion system (T6SS) is a multiprotein machine that delivers protein effectors in both prokaryotic and eukaryotic cells, allowing interbacterial competition and virulence. The mechanism of action of the T6SS requires the contraction of a sheath-like structure that propels a needle towards target cells, allowing the delivery of protein effectors. Here, we provide evidence that the entero-aggregative *Escherichia coli* Sci-1 T6SS is required to eliminate competitor bacteria. We further identify Tle1, a toxin effector encoded by this cluster and showed that Tle1 possesses phospholipase A_1 and A_2 activities required for the interbacterial competition. Self-protection of the attacker cell is secured by an outer membrane lipoprotein, Tli1, which binds Tle1 in a 1:1 stoichiometric ratio with nanomolar affinity, and inhibits its phospholipase activity. Tle1 is delivered into the periplasm of the prey cells using the VgrG1 needle spike protein as carrier. Further analyses demonstrate that the C-terminal extension domain of VgrG1, including a transthyretin-like domain, is responsible for the interaction with Tle1 and its subsequent delivery into target cells. Based on these results, we propose an additional mechanism of transport of T6SS effectors in which cognate effectors are selected by specific motifs located at the C-terminus of VgrG proteins.

Accepted 26 November, 2015. *For correspondence. E-mail ljournet@imm.cnrs.fr; Tel. 33491164156; Fax 33491712124. †Present address: Laboratoire des Sciences de l'Environnement Marin (LEMAR), Institut Universitaire Européen de la Mer (IUEM), Université de Bretagne Occidentale, CNRS, IRD, Ifremer – UMR 6539, Technopôle Brest Iroise, 29280, Plouzané, France.

Introduction

The T6SS is built by the assembly of at least 13 proteins encoded by usually clustered genes. A transmembrane complex anchors to the cell envelope a phage-like tail complex that extends from the membrane in the cytoplasm (Coulthurst, 2013; Ho *et al.*, 2014; Zoued *et al.*, 2014; Basler, 2015). The membrane complex serves as docking station for assembly of the tail complex (Durand *et al.*, 2015), a dynamic tubular structure functionally and structurally homologous to the contractile tail of bacteriophages (Bönemann *et al.*, 2009; Leiman *et al.*, 2009; Bönemann *et al.*, 2010; Basler *et al.*, 2012). It is constituted of an inner tube made of stacked hexameric rings of the Hcp protein, whose three-dimensional structure is very similar to that of the bacteriophage tail tube gpV (Mougous *et al.*, 2006; Pell *et al.*, 2009; Ballister *et al.*, 2008; Brunet *et al.*, 2014; Douzi *et al.*, 2014). This Hcp edifice resembles a channel-like tubular structure with a 40-Å internal diameter and is surrounded by a contractile sheath made of the TssB and TssC proteins (Kudryashev *et al.*, 2015). The inner tube/sheath structure is built on an assembly platform – the baseplate – that contacts the membrane

complex (Brunet *et al.*, 2015). The TssBC sheath is highly dynamic. Cycles of sheath assembly, contraction and disassembly were visualized by time-lapse fluorescence microscopy using fluorescent TssB–sfGFP fusion constructs (Basler *et al.*, 2012; Brunet *et al.*, 2013; Kapitein *et al.*, 2013). The inner tube is capped by the spike composed of a VgrG (valine glycine repeat protein) trimer. This complex is structurally homologous to the bacteriophage T4 gp27-gp5 cell-puncturing device (Leiman *et al.*, 2009). The VgrG trimer global fold consists of a gp27-like trimer, followed by the N-terminal OB fold domain of gp5 and a three-stranded β-helix that forms the needle of the spike complex. In some T6SSs, an additional component called PAAR (Pro-Ala-Ala-Arg motif-containing protein) assembles a conical structure at the tip of the VgrG protein (Shneider *et al.*, 2013). This component was proposed to sharpen the VgrG spike, to assist folding and to stabilize the β-helix domain of VgrG or to be used as an adaptor component mediating interaction between VgrG and effector proteins (Shneider *et al.*, 2013). The contractile structure assembles in an elongated metastable state. Upon contact with a target cell, the sheath contraction is thought to propel the Hcp inner tube towards the target cell, piercing the membrane using the VgrG/PAAR spike complex, hence leading to effector delivery (Cascales, 2008; Silverman *et al.*, 2012; Coulthurst, 2013; Ho *et al.*, 2014; Zoued *et al.*, 2014). In agreement with this mechanism of action, time-lapse fluorescence recordings demonstrated that contraction of the sheath is correlated with lysis of the prey cell (Brunet *et al.*, 2013).

The T6SS is a versatile machinery as it has been shown to have roles in both pathogenesis and interbacterial competition, and effectors that have eukaryotic or prokaryotic targets have been identified and characterized (Durand *et al.*, 2014; Russell *et al.*, 2014; Alcoforado Diniz *et al.*, 2015). For examples, the *Vibrio cholerae* and *Aeromonas hydrophila* T6SSs disable eukaryotic cells by delivering specific effector modules that interfere with the actin cytoskeleton dynamics (Pukatzki *et al.*, 2006; Pukatzki *et al.*, 2007; Suarez *et al.*, 2010; Durand *et al.*, 2012) while a growing number of T6SSs have been demonstrated to have antibacterial activities (Hood *et al.*, 2010; MacIntyre *et al.*, 2010; Schwarz *et al.*, 2010; Murdoch *et al.*, 2011; Brunet *et al.*, 2013; Carruthers *et al.*, 2013; Gueguen and Cascales, 2013). In fact, bacteria do not live alone in their environment: they share the same ecological niche, socialize, but also display antagonistic behaviours and compete with each other. The T6SS is one of the key players during the bacterial warfare by delivering antibacterial effectors directly into bacterial competitor cells (Coulthurst, 2013; Durand *et al.*, 2014; Ho *et al.*, 2014; Alcoforado Diniz *et al.*, 2015). Among these effectors, the Tae (type VI secretion amidase effector) and Tge (type VI secretion glycoside hydrolase effector) effectors degrade the peptidoglycan of the target cells, the Tle (type VI lipase effectors) toxins hydrolyse the membrane phospholipids of the target cells whereas the Tde (type VI DNase effectors) are nucleases (Benz and Meinhart, 2014; Durand *et al.*, 2014; Russell *et al.*, 2014). Recently, the *Pseudomonas aeruginosa* Tse6 T6SS effector has been demonstrated to have NAD(P)+ glycohydrolase activity, hence depleting the NAD(P)+ pool of the target cell (Whitney *et al.*, 2015). The cell wall degrading effectors target the peptide stem (Tae) or the glycan strands (Tge) of the peptidoglycan and can be divided in several families with different hydrolysed bond specificities (Benz and Meinhart, 2014; Durand *et al.*, 2014; Russell *et al.*, 2014). Tle toxins consist to a large group of enzymes that could be divided into five divergent families bearing phospholipase A_1, A_2 or D activities (Russell *et al.*, 2013). Interestingly, whereas the Tae and Tge toxins are antibacterial only, members of the Tle or Tde toxin families target macromolecules present in both eukaryotic and prokaryotic cells. Indeed, a number of Tle toxins have been shown to cause damages in eukaryotic cells, such as the *P. aeruginosa* PldB ($Tle5b^{PA}$) protein that promotes invasion of eukaryotic cells by activation of the AKT/PI3pathway (Jiang *et al.*, 2014) or the $Tle2^{VC}$ toxin that is necessary for *V. cholerae* to escape amoeba predation (Dong *et al.*, 2013).

To prevent self-intoxication, Tae, Tge, Tle and Tde antibacterial effectors are produced concomitantly with cognate immunity proteins, called Tai, Tgi, Tli and Tdi respectively (Benz and Meinhart, 2014; Durand *et al.*, 2014; Russell *et al.*, 2014). Usually, the immunity protein resides in the compartment in which the toxin is delivered, binds to the toxin with high (nanomolar) affinity and inhibits it, either by the occlusion of the catalytic site or by preventing access to its target (Benz and Meinhart, 2014; Durand *et al.*, 2014; Russell *et al.*, 2014).

T6SS toxins exist either as independent proteins or additional modules fused to the Hcp, VgrG or PAAR components. These effector modules are hence delivered into the target cell upon sheath contraction. The cargo mechanisms by which independent effectors are delivered into the target cell is less known. The current transport models propose that these effectors bind to the Hcp, VgrG or PAAR proteins directly or via adaptor proteins, and therefore, that these structural components of the machine are used as carriers (Shneider *et al.*, 2013; Silverman *et al.*, 2013; Durand *et al.*, 2014; Hachani *et al.*, 2014). Indeed, the *P. aeruginosa* Tae1 and Tge1 effectors are embedded into the lumen of the Hcp ring and are stored into the Hcp inner tube before sheath contraction (Silverman *et al.*, 2013). It has been

suggested that several *P. aeruginosa* effectors bind directly or indirectly to VgrG (Dong *et al*., 2013; Hachani *et al*., 2014; Whitney *et* al., 2014). Hachani *et al*. suggested that VgrG/effector combinations are not interchangeable and that selection of the effector depends on specific motifs on VgrG (Hachani *et al*., 2014). More recently, conserved T6SS adaptor proteins linking VgrG and cognate effectors were identified (Alcoforado Diniz and Coulthurst, 2015; Liang *et al*., 2015; Unterweger *et al*., 2015).

In the recent years, we have characterized the regulatory mechanisms and the structural architecture of the entero-aggregative *Escherichia coli* (EAEC) Sci-1 Type VI secretion system (T6SS-1). However, the function of this T6SS has remained elusive and no T6SS-1 substrate has been identified. The EAEC *sci-1* gene cluster encodes the 13 core components, a PAAR protein, the TagL accessory protein and 6 genes of unknown function (Journet and Cascales, 2016). Among these genes, a gene encoding a putative Tle1 effector followed by a gene encoding a putative lipoprotein is found downstream *vgrG1*. In this study, we demonstrate that the Sci-1 T6SS is required for EAEC antibacterial activity in minimal medium and that $Tle1^{EAEC}$ possesses phospholipase A_1 (PLA_1) and A_2 (PLA_2) activities responsible for the antibacterial activity of Sci-1 T6SS. We then show that $Tli1^{EAEC}$ is an outer membrane immunity lipoprotein that binds tightly to $Tle1^{EAEC}$ and inhibits its PLA activity. Finally, we demonstrate that $Tle1^{EAEC}$ is a cargo effector and is delivered into target cells using the VgrG1 spike as carrier through direct interaction with the VgrG1 C-terminal extension.

Results

The EAEC T6SS sci-1 *gene cluster has antibacterial activity in minimal medium*

To gain insights into the function of the Sci-1 T6SS, we compared the EAEC 17-2 wild-type (WT) strain with its derivative strain deleted of the entire *sci-1* gene cluster (Δ*T6SS-1*) for (i) virulence towards eukaryotic cells using the *Cænorhabditis elegans* model of infection and (ii) antagonism against competitor bacteria. The experiments were performed in NGM or *sci-1* inducing minimal media (SIM) to allow maximal expression of the *sci-1* gene cluster (Brunet *et al*., 2011). In these conditions, the growth rates of the WT strain and its isogenic Δ*T6SS-1* mutant were comparable (data not shown).

In *C. elegans*, the WT EAEC 17-2 cells were moderately virulent, with a lethal dose 50% (LD_{50}) of 7 days (compared to 3 days for *Burkholderia cenocepacia* K56-2). Identical values were obtained when Δ*T6SS-1* cells were used as feeding source for the worms (Fig. 1A).

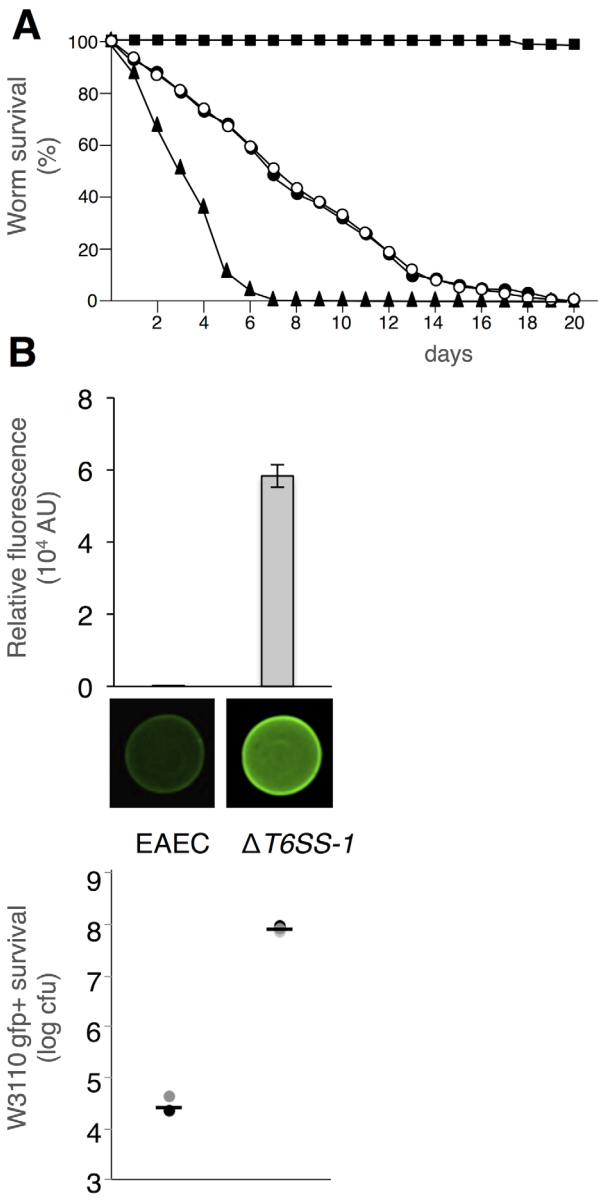

Fig. 1. The *sci-1* T6SS gene cluster contributes to EAEC antibacterial activity.
A. The EAEC *sci-1* T6SS is not required for virulence towards the *C. elegans* model of infection. The number of nematods surviving on lawn of the indicated strain (closed squares, OP50; closed circles, EAEC 17-2; open circles, EAEC Δ*T6SS-1*; closed triangles, *B. cenocepacia* K56-2) was plotted as percentage (% survival) over time (days).
B. Antibacterial assay. Prey cells (W3110 gfp^+, kan^R) were mixed with the indicated attacker cells, spotted onto *sci-1*-inducing medium (SIM) agar plates and incubated for 4 h at 37°C. The image of a representative bacterial spot is shown and the relative fluorescent levels (in AU) are indicated in the upper graph. The number of recovered *E. coli* prey cells is indicated in the lower graph (in $\log_{10}$ of cfu). The circles indicate values from three independent assays, and the average is indicated by the bar.

These data suggest that the T6SS-1 is not involved in the virulence of EAEC 17-2 in the *C. elegans* model of infection. The antibacterial activity was then tested in

SIM. The *E. coli* K-12 strain W3110 (devoid of T6SS genes) engineered to constitutively produce the green fluorescent protein (GFP) and to resist kanamycin was used as prey. Attacker and prey cells were mixed in a 4:1 ratio and the mixtures were spotted on SIM agar plates. After a 4-hour incubation at 37°C, the fluorescence levels and the number of kanamycin-resistant colony-forming units (cfu) were measured to estimate the survival of the prey cells (Fig. 1B). In these conditions, the deletion of the *sci-1* gene cluster increased the recovery of prey cells. We therefore concluded that the T6SS-1 machine provides antibacterial activity in minimal medium.

The EC042_4534 *gene product encodes an antibacterial effector with phospholipase A_1 and A_2 activities*

To identify potential effector toxins, we screened the *sci-1* gene cluster. The *sci-1* gene cluster encodes the 13 T6SS core-components, *PAAR* and a number of genes of unknown function (Fig. 2A). Among those, a group of three genes, *EC042_4534*, *EC042_4535* and *EC042_4536* is found between the *vgrG1* (*EC042_4533*) and *PAAR* (*EC042_4537*) genes. *EC042_4534* [NCBI Gene Identifier (GI): 284924255] is encoded directly downstream *vgrG1*. Computer analysis of the *EC042_4534* gene product using Pfam predicts it carries a DUF2235 domain (uncharacterized α/β hydrolase domain, amino-acid 36 to 333, E-value 9.7 e-24). A phylogenetic reconstruction of EC042_4534 with members of Type VI lipase effector (Tle) families 1–5 (as defined by Russell *et al.*, 2013) showed that EC042_4534 segregates with Tle1 members (Supporting Information Fig. S4). Multiple alignments of EC042_4534 with Tle1 members revealed the characteristic GXSXG motif usually found in lipases and some phospholipases (Supporting Information Fig. S5). Fold recognition servers (such as Phyre2, Kelley and Sternberg, 2009) suggest significant homologies between EC042_4534 and the D1 catalytic domain of the *P. aeruginosa* $Tle1^{PA}$ protein (Hu *et al.*, 2014). The structure of EC042_4534 was therefore modelled using the structure of $Tle1^{PA}$ (Protein Data Bank (PDB) identifier 4O5P, Hu *et al.*, 2014) as template (Fig 2B). As expected, the structural model predicts that the catalytic triad is composed of the Ser-197, Asp-245 and His-310 amino acids (Fig. 2B). The EC042_4534 protein is thus a putative member of the Tle1 family of T6SS effectors and was named hereafter $Tle1^{EAEC}$.

In order to biochemically characterize $Tle1^{EAEC}$, its coding sequence was cloned into the pETG20A *E. coli* expression vector, fused to a N-terminal hexahistidine-tagged thioredoxin domain followed by a Tobacco Etch Virus (TEV) cleavage site. The WT $Tle1^{EAEC}$ protein ($Tle1^{EAEC(WT)}$) and a variant bearing a mutation in the putative catalytic triad ($Tle1^{EAEC(S197A)}$) were purified to homogeneity using ion metal affinity chromatography and gel filtration, and the recombinant $Tle1^{EAEC(WT)}$ and $Tle1^{EAEC(S197A)}$ proteins were obtained upon cleavage using the TEV protease (see inset in Fig. 2C). Since the two Tle1 family members characterized so far, *B. thailandensis* $Tle1^{BT}$ and $Tle1^{PA}$, have phospholipase A_2 (PLA_2) activity (Russell *et al*, 2013; Hu *et al.*, 2014), the activity of the purified $Tle1^{EAEC}$ and $Tle1^{EAEC(S197A)}$ were tested on fluorogenic phospholipid substrates (Fig. 2C). $Tle1^{EAEC}$ possesses both phospholipase A_1 (PLA_1) activity (specific activity (SA) = 1338 pmole min^{-1} mg^{-1}) and a 12.5 lower PLA_2 activity (SA = 107 pmole min^{-1} mg^{-1}). By contrast, the purified Tle1 protein has undetectable phospholipase C and triacylglycerol lipase activities (data not shown). The PLA_1 and PLA_2 activities were abolished when the putative catalytic Ser-197 residue was substituted by an alanine (S197A mutant) (Fig. 2C). Finally, to gain insight into $Tle1^{EAEC}$ specificity, the rate of hydrolysis of major lipids of bacterial membranes phosphatidylethanolamine (DLPE) and phosphatidylglycerol (DLPG), as well as phosphatidylcholine (DLPC) and phosphatidylserine (DLPS), was tested on monolayer films (Table 1). $Tle1^{EAEC}$ – but not its S197A mutant – shows a slight activity on DLPC, DLPE and DLPS while DLPG hydrolysis was undetectable. Based on bioinformatic analyses and biochemical results, we conclude that the EC042_4534 protein is a member of the Tle1 family of T6SS effectors having PLA_1/PLA_2 activity.

In order to test whether $Tle1^{EAEC}$ was involved in the antibacterial activity of the Sci-1 T6SS, we constructed a *tle1* deletion mutant strain. Due to technical genetic constraints (see Experimental Procedures), this strain is also deleted of the following *tli1* gene (that encodes its cognate immunity, see below). The Hcp release assay, which reflects proper assembly and function of the T6SS, demonstrated that Tle1 (and Tli1) is not necessary for T6SS assembly and function (Supporting Information Fig S1). However, as shown in Fig. 2D, the absence of Tle1 and Tli1 decreased the antibacterial activity of EAEC against *E. coli* K-12 cells to the same extent as the T6SS-1 deletion mutant. The antibacterial activity was restored by the *trans*-expression of WT *tle1*, but not with that of $tle1^{S197A}$ (Fig. 2D). Therefore, these results suggest that the antibacterial toxicity of the *sci-1* T6SS gene cluster towards *E. coli* is conferred by the phospholipase activity of $Tle1^{EAEC}$.

$Tli1^{EAEC}$ *(EC042_4535) assures self-protection by inhibiting* $Tle1^{EAEC}$ *phospholipase activity*

In T6SS, protection against kin cells is secured by the production of immunity proteins that specifically bind

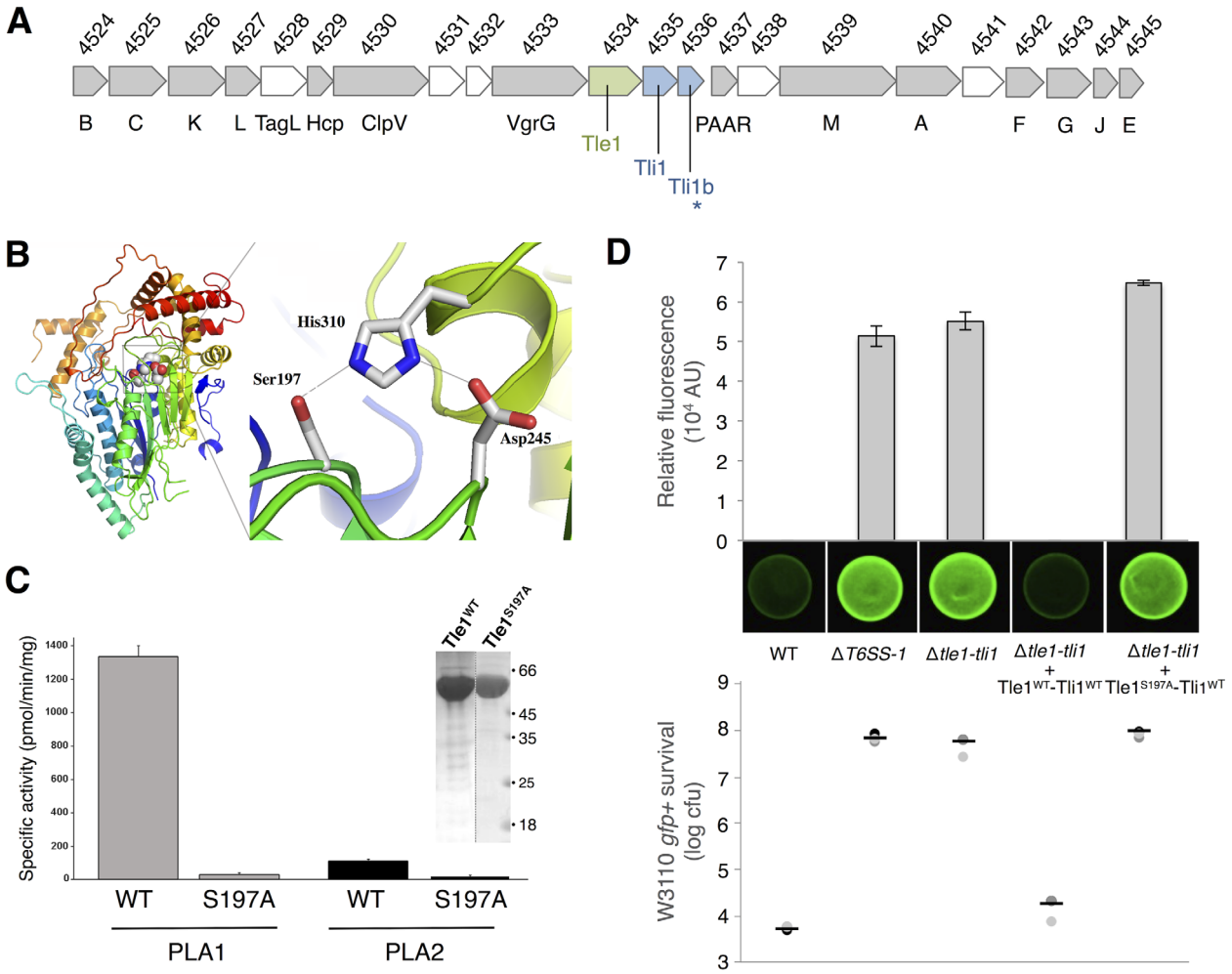

Fig. 2. EC042_4534 phospholipase activity is responsible for Sci-1-mediated antibacterial activity.
A. Schematic representation of the EAEC 17-2 *sci-1* T6SS gene cluster. The numbers on top refer to the genes locus tag (EC042_XXXX). Genes encoding core components (identified by their names on bottom) are coloured grey. Genes of unknown function are indicated in white. The *EC042_4534* gene encoding Tle1 is indicated in green whereas the two genes encoding the Tli1 and Tli1b immunity proteins are coloured in blue. The asterisk below Tli1b indicates that a frameshift mutation on the 17-2 chromosome yields a truncated protein (Supporting Information Fig. S2).
B. Homology-based structural model of EC042_4534 based on the crystal structure of the *P. aeruginosa* $Tle1^{PA}$ effector (PDB: 4O5P). The magnification highlights the positions and orientations of the putative catalytic triad amino-acid side chains (Ser-197, Asp-245 and His-310).
C. Specific phospholipase A_1 (PLA_1) and A_2 (PLA_2) activity measurements of the EC042_4534 $Tle1^{EAEC}$ WT and S197A mutant proteins using fluorescent phospholipids. Specific activities were calculated from the velocity slope obtained for 25 min using 20 μg of purified protein. Data are expressed as mean values ± standard deviations of three independent assays (CV% < 5%). The SDS-PAGE analysis of the purified EC042_4534 ($Tle1^{WT}$) and S197A ($Tle1^{S197A}$) proteins (40 μg) after Coomassie blue staining is shown in the inset (molecular weight markers (in kDa) are indicated on the right).
D. EC042_4534 ($Tle1^{EAEC}$) phospholipase activity is responsible for Sci-1-mediated antibacterial activity. The antibacterial activity was assessed by mixing W3110 *gfp*$^+$ prey cells with the indicated attacker cells for 4 h at 37°C in *sci-1*-inducing medium containing 0.02% arabinose (WT (EAEC 17-2), Δ*T6SS-1* (*sci-1* gene cluster deletion derivative) and Δ*tle1-tli1* (17-2 deleted of the *tle1* and *tli1* genes) carrying the pBAD18 empty vector, or Δ*tle1-tli1* producing WT Tle1 ($Tle1^{WT}$) and Tli1 or the S197A Tle1 mutant ($Tle1^{S197A}$) and Tli1 from the pBAD18-Tle1-Tli1 or pBAD18-$Tle1^{S197A}$-Tli1 respectively). The image of a representative bacterial spot is shown and the relative fluorescent levels (in AU) are indicated in the upper graph. The number of recovered *E. coli* prey cells is indicated in the lower graph (in $\log_{10}$ of cfu). The circles indicate values from three independent assays, and the average is indicated by the bar.

and inhibit their cognate toxins. Usually, effector/immunity genes are found in tandem in genomes. In the *sci-1* gene cluster, the *tle1*^{EAEC} gene is followed by a duplicated region encoding two putative immunity proteins: *EC042_4535* and *EC042_4536* (GIs: 284924256 and 284924257 respectively). In the sequenced 042 strain, the 225-amino-acid EC042_4535 and EC042_4536 proteins only differ by a few residues at their extreme C-termini (Supporting Information Fig. S2A). However, in the 17-2 strain used in this study, the *EC042_4536* gene

Table 1. Rates of hydrolysis of DLPC, DLPE, DLPS and DLPG monolayers at a constant surface pressure of 20 mN m^{-1}.

Phospholipid substrates	Enzyme activity (μmole cm^{-2} min^{-1} M^{-1}) Tle1	$Tle1_{S197A}$	Tle1 + Tli1 (1:2 mol/mol)
DLPC	148 (± 9)	*No activity*	*No activity*
DLPE	109 (± 5)	*No activity*	*No activity*
DLPS	97 (± 4)	*No activity*	*No activity*
DLPG	*No activity*	*No activity*	*No activity*

Assays were carried out in a 'zero order' trough as described in the Experimental Procedures section. The final concentration of Tle1 and $Tle1_{S197A}$ was 11 nM for the lipolysis of each phospholipid. Enzyme activities are expressed as the number of moles of substrate hydrolysed by time unit and surface unit of the reaction compartment of the 'zero order' trough for an arbitrary lipase concentration of 1 M. All data are presented as mean values ± standard deviations of at least 2 independent assays (CV% < 6%). Buffer: 10 mM Tris (pH 8.0), 100 mM NaCl, 21 mM $CaCl_2$ and 1 mM EDTA.

has a frameshift mutation at nucleotide 386 that yields a 154-amino-acid truncated protein (Supporting Information Figs S2A and S2B) that was not further analysed. To test if the product of the *EC042_4535* gene assures protection against $Tle1^{EAEC}$, the *EC042_4535* gene was expressed from the pBAD18 vector in W3110 *gfp*$^+$ reporter prey cells. Antibacterial competition experiments showed that the production of EC042_4535 in the *E. coli* K-12 prey conferred full protection against the antibacterial activity of the Sci-1 T6SS (Fig. 3A). In addition to showing that EC042_4535 confers protection, this result also demonstrates that $Tle1^{EAEC}$ is delivered into target cells and suggests that $Tle1^{EAEC}$ is the major antibacterial Sci-1 T6SS effector in these conditions. In agreement with this result, when used as prey, the Δ*EC042_4535-4536* mutant was killed by the WT EAEC but not by the Δ*T6SS-1* or the *tle1-tli1* deletion mutant strain (Fig. 3B). Finally, production of EC042_4535 in Δ*EC042_4535-4536* prey cells protected them against EAEC killing. It is worthy to note that the recovered fluorescence of complemented Δ*EC042_4535-4536* cells is higher than in noncomplemented cells, likely due to the sickness of the Δ*EC042_4535-4536* prey cells (Fig. 3B). To confirm this result biochemically, the EC042_4535 protein was purified to homogeneity and tested for its ability to interfere with the $Tle1^{EAEC}$ activity. Figure 3C and Table 1 show that the $Tle1^{EAEC}$ phospholipase activity was inhibited by EC042_4535 in a dose-dependent manner. Interestingly, the $Tle1^{EAEC}$ activity

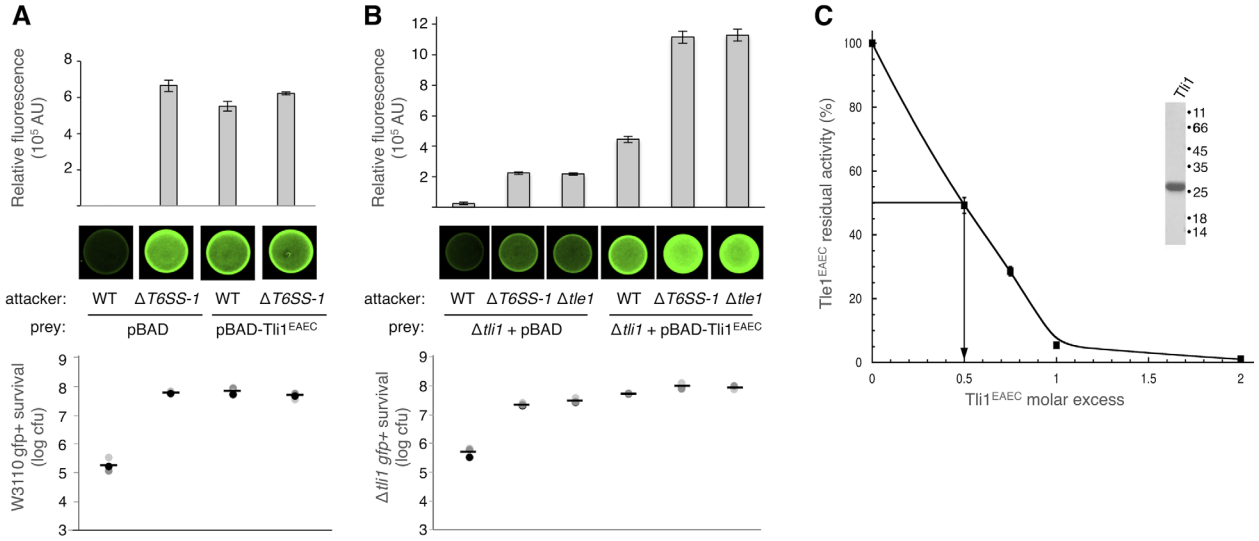

Fig. 3. $Tli1^{EAEC}$ inhibits $Tle1^{EAEC}$ antibacterial phospholipase activity.
A. Antibacterial assay. The antibacterial activity was assessed by mixing W3110 *gfp*$^+$ prey cells producing (pBAD-$Tli1^{EAEC}$) or not (pBAD18) the EC042_4535 ($Tli1^{EAEC}$) protein from the pBAD promoter with the indicated attacker cells for 4 h at 37°C in *sci-1*-inducing medium containing 0.02% arabinose. The image of a representative bacterial spot is shown and the relative fluorescent levels (in AU) are indicated in the upper graph. The number of recovered *E. coli* prey cells is indicated in the lower graph (in $\log_{10}$ of cfu). The circles indicate values from three independent assays, and the average is indicated by the bar.
B. The antibacterial activity was assessed by mixing Δ*tli1-tli1b* (17-2 deleted of the *tli1* and *tli1b* genes) *gfp*$^+$ prey cells producing (pBAD-$Tli1^{EAEC}$) or not (pBAD18) the EC042_4535 ($Tli1^{EAEC}$) protein from the pBAD promoter with the indicated attacker cells for 4 h at 37°C in *sci-1*-inducing medium containing 0.02% arabinose. The image of a representative bacterial spot is shown and the relative fluorescent levels (in AU) are indicated in the upper graph. The number of recovered *E. coli* prey cells is indicated in the lower graph (in $\log_{10}$ of cfu). The circles indicate values from three independent assays, and the average is indicated by the bar.
C. $Tli1^{EAEC}$ inhibition of $Tle1^{EAEC}$ PLA_1 activity. The rate of hydrolysis of PED-A_1 by purified $Tle1^{EAEC}$ at 20°C in presence of increasing concentrations of $Tli1^{EAEC}$ was plotted against the molar excess of $Tli1^{EAEC}$. The SDS-PAGE analysis of the purified $Tli1^{EAEC}$ (Tli1) protein after Coomassie blue staining is shown in the inset [molecular weight markers (in kDa) are indicated on the right].

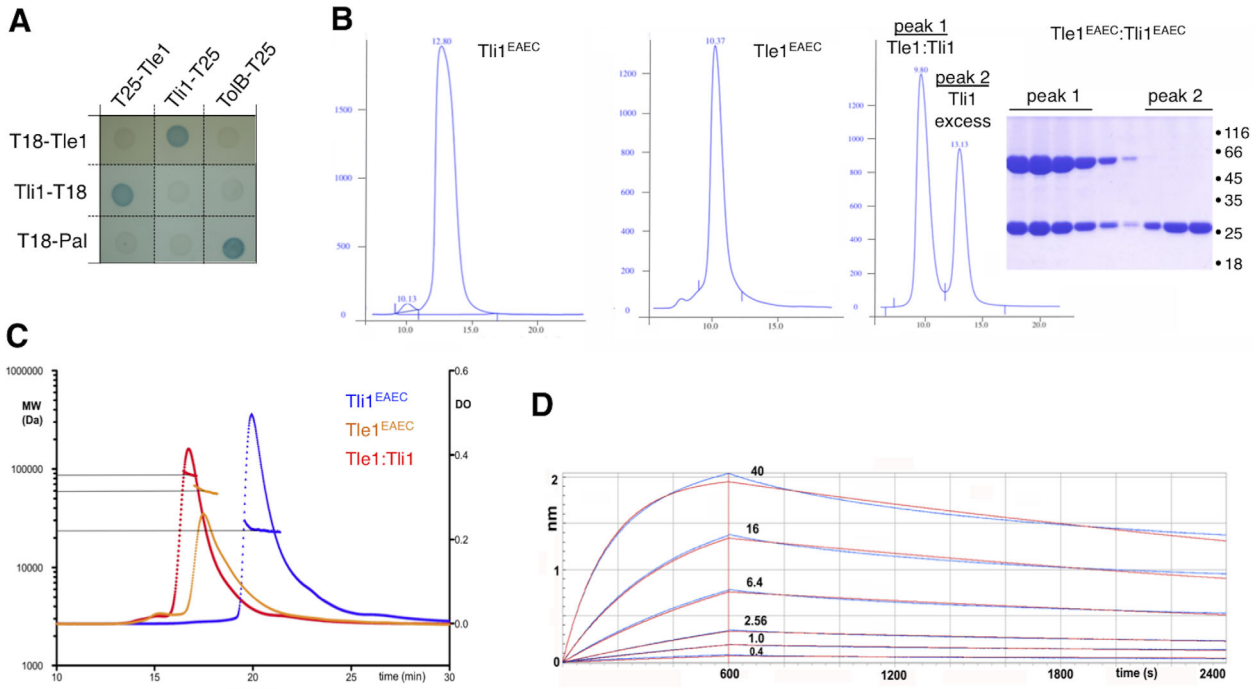

Fig. 4. $Tli1^{EAEC}$ binds $Tle1^{EAEC}$ with nanomolar affinity.
A. Bacterial two-hybrid analysis. BTH101 reporter cells producing the indicated $Tle1^{EAEC}$ (Tle1) or $Tli1^{EAEC}$ (Tli1) proteins fused to the T18 or T25 domain of the *Bordetella* adenylate cyclase were spotted on X-Gal indicator plates. The blue colour of the colony reflects the interaction between the two proteins. Controls include T18 and T25 fusions to TolB and Pal, two proteins that interact but unrelated to the T6SS.
B. Gel filtration analysis on a calibrated Superdex 75 (10/30) column. The purified $Tli1^{EAEC}$ (left panel), $Tle1^{EAEC}$ (middle panel) proteins and the $Tle1^{EAEC}$/$Tli1^{EAEC}$ mixture (right panel) were separated by gel filtration. $Tli1^{EAEC}$, $Tle1^{EAEC}$ and the $Tle1^{EAEC}$-$Tli1^{EAEC}$ complex eluted at 12.8 ml (~ 24 kDa), 10.37 ml (~ 66 kDa) and 9.8 ml (~ 82 kDa) respectively. The inset is the SDS-PAGE and Coomassie blue staining analysis of the fractions eluted after $Tle1^{EAEC}$-$Tli1^{EAEC}$ complex separation. Peak 1 contains the two proteins whereas peak 2 (13.1 ml) contains the excess of $Tli1^{EAEC}$. The molecular weight markers (in kDa) are indicated on the right.
C. MALS/QELS/UV/RI analysis. The UV absorbance at 280 nm corresponding to $Tli1^{EAEC}$ (blue line), $Tle1^{EAEC}$ (orange line) and to the $Tle1^{EAEC}$-$Tli1^{EAEC}$ complex (red line) was plotted against time (min. after sample injection in the High Performance Liquid Chromatography system). The traces indicating the molar mass (indicated on the left, in Da) are shown on each peak.
D. Bio-layer interferometry analysis. Recordings of the binding of purified $Tle1^{EAEC}$ [concentrations (in nM) indicated above the corresponding curve] to the streptavidin chip coupled to biotinylated $Tli1^{EAEC}$. The response (in nm) is plotted versus the time (in seconds). The experimental association and dissociation curves (blue) are compared to the simulated ones (red). The calculated K_D value is 1.50 ± 0.05 nM.

was completely abolished with a $Tle1^{EAEC}$:EC042_4535 molecular ratio of 1:1 (Fig. 3C), which is the highest ratio that can be expected between an enzyme and a specific inhibitor. Taken together, these results confirm that EC042_4535 is an immunity protein that protects against the phospholipase activity of $Tle1^{EAEC}$, and therefore, EC042_4535 was named $Tli1^{EAEC}$.

$Tli1^{EAEC}$-dependent $Tle1^{EAEC}$ inhibition is mediated by tight binding of $Tli1^{EAEC}$ to $Tle1^{EAEC}$

The $Tli1^{EAEC}$-mediated inhibition of $Tle1^{EAEC}$ activity strongly suggests that $Tli1^{EAEC}$ binds to $Tle1^{EAEC}$. To test this hypothesis, we first performed a bacterial two-hybrid (BACTH) assay. The sequence encoding $Tle1^{EAEC}$ was cloned downstream the T18 or T25 domains of the *Bordetella* adenylate cyclase, whereas the sequence encoding $Tli1^{EAEC}$ (deleted of its lipoprotein signal sequence) was cloned upstream the T18 and T25 domains. When the $Tle1^{EAEC}$ and $Tli1^{EAEC}$ fusion proteins were co-produced, the expression of the reporter gene was activated demonstrating that $Tli1^{EAEC}$ and $Tle1^{EAEC}$ interact (Fig. 4A). The BACTH assay also suggested that $Tle1^{EAEC}$ and $Tli1^{EAEC}$ are monomeric as no Tle1-Tle1 or Tli1-Tli1 interactions were detected (Fig. 4A). To validate these results by alternative approaches, the purified $Tle1^{EAEC}$ and $Tli1^{EAEC}$ proteins, and the mixture of the two purified proteins, were subjected to gel filtration and online multiangle laser light scattering/quasielastic light scattering/absorbance/refractive index (MALS/QELS/UV/RI). Size exclusion chromatography (SEC) demonstrated that $Tle1^{EAEC}$ and $Tli1^{EAEC}$ have apparent molecular masses of 66 kDa and 23.9 kDa respectively (Fig. 4B). These values, in agreement with their theoretical molecular weights of 62.3 and 24 kDa, further indicate that these proteins are

monomeric in solution. Analysis of the Tle1^{EAEC}/Tli1^{EAEC} mixture showed the apparition of an additional peak containing both proteins (peak 1, Fig. 4B), demonstrating complex formation between the two proteins *in vitro*. With an apparent molecular mass of ~ 82 kDa, this complex likely corresponds to a Tle1^{EAEC}-Tli1^{EAEC} heterodimer (calculated molecular weight: 86 kDa). Analyses of purified Tle1^{EAEC}, Tli1^{EAEC} and Tle1^{EAEC}-Tli1^{EAEC} complex by MALS/QELS/UV/RI confirmed that both Tle1^{EAEC} and Tli1^{EAEC} are monomeric and that the Tle1^{EAEC}-Tli1^{EAEC} complex has a 1:1 stoichiometry (Fig. 4C). To determine the strength of the Tle1^{EAEC}-Tli1^{EAEC} interaction, the association of the two partners was monitored by Biolayer Interferometry (BLI). The Tli1^{EAEC} protein was biotinylated, coupled to a streptavidin sensortip and the association and dissociation of Tle1^{EAEC} were recorded for 600 and 1800 s respectively (Fig. 4D). Based on the curve fitting and assuming a 1:1 Tle1^{EAEC}:Tli1^{EAEC} heterodimer, Tle1^{EAEC} and Tli1^{EAEC} associates with a K_D constant value of 1.5 ± 0.05 nM. The K_{on} and K_{off} values ($K_{on} = 1.65 \times 10^5$ M^{-1} s^{-1} and $K_{off} = 2.2 \times 10^{-4}$ s^{-1}) are in agreement with a rapid association of the two proteins, but a slow dissociation of the complex. Taken together, these results demonstrate that Tle1^{EAEC} and Tli1^{EAEC} are monomeric in solution and interact to form a stable 1:1 heterodimer with nanomolar affinity.

Tli1^{EAEC} is an outer membrane lipoprotein protecting against delivery of cytoplasmic Tle1^{EAEC} in the periplasm of target cells

The *tle1^{EAEC}* gene is predicted to encode a 62.3-kDa cytoplasmic protein, with no predicted signal peptide or trans-membrane segment. Fractionation of EAEC cells producing Tle1^{EAEC} fused to a C-terminal VSVG epitope (Tle1$_{VSVG}$) showed that Tle1^{EAEC} co-localizes with the EF-Tu cytoplamic marker hence confirming its cytoplasmic localization (Fig. 5A). Tle1$_{VSVG}$ was not detected in the supernatant fraction (data not shown). By contrast, the *tli1^{EAEC}* gene is predicted to encode a protein with a signal sequence bearing a characteristic lipobox motif, such as other Tli1 homologues (Fig. 5B). In agreement with this prediction, Tli1^{EAEC} processing was inhibited by the signal peptidase II (SPII) inhibitor globomycin (Fig. 5C). In Gram-negative bacteria, lipoprotein sorting is controlled by the Lol complex and the final localization of the lipoprotein follows the '+2 rule', i.e. depends on the residue immediately downstream the acylated cysteine (Zückert, 2014). In Tli1^{EAEC}, the +2 residue is an asparagine suggesting an outer membrane destination (Fig. 5B). To determine its subcellular localization, total membranes of *tli1^{EAEC}* cells producing a functional C-terminally FLAG-tagged Tli1^{EAEC} protein (Tli1$_{FL}$) were subjected to sedimentation density sucrose gradient separation. By comparison with the behaviour of control proteins in the sucrose gradient (the outer membrane porin OmpF and the inner membrane NADH oxidase), we concluded that Tli1^{EAEC} co-fractionates with outer membrane proteins (Fig. 5D). Taken together these experiments defined that Tle1^{EAEC} is a cytoplasmic protein whereas Tli1^{EAEC} is an outer membrane lipoprotein.

To explain the interaction between Tle1^{EAEC} and Tli1^{EAEC} despite their different localization, we predicted that Tle1^{EAEC} should be delivered into the periplasm of the target cell, and thus be a periplasmic-acting toxin. To test this hypothesis, we tested the effects of the heterologous production of Tle1^{EAEC} in the cytoplasm or periplasm of *E. coli* K-12. Tle1^{EAEC} was readily produced in the cytoplasm of *E. coli* without any toxic effect (Fig. 6A). By constrast, we did not succeed to construct a vector allowing the artificial periplasmic production of Tle1^{EAEC} by fusing the *tle1^{EAEC}*-coding sequence downstream the *ompA* signal sequence (sp-Tle1^{EAEC}). The construction was only obtained when the cloning steps were performed in cells producing Tli1^{EAEC} from the pBAD33 vector in the presence of arabinose. Indeed, periplasmic targeting of Tle1^{EAEC} is highly toxic in the absence of arabinose (Fig. 6B). The sp-Tle1^{EAEC} toxicity is efficiently counteracted by the co-production of Tli1^{EAEC}. In agreement with the *in vitro* and *in vivo* studies (Fig. 2C and D), the periplasmic production of the Tle1^{EAEC} catalytic mutant Tle1^{S197A} had roughly no effect on cell viability (Fig. 6B), confirming that Tle1^{EAEC} bacterial toxicity is conferred by its catalytic activity.

Tle1^{EAEC} interacts with the VgrG1 C-terminal extension

The cargo model proposes that independent effectors are secreted through direct or indirect (via adaptor proteins) interactions with VgrG, Hcp or PAAR protein components (Shneider *et al.*, 2013; Silverman *et al.*, 2013; Durand *et al.*, 2014; Hachani *et al.*, 2014; Whitney *et al.*, 2014; Alcoforado Diniz and Coulthurst, 2015; Liang *et al.*, 2015; Unterweger *et al.*, 2015). Bioinformatic analyses of the *sci-1* genes of unknown function showed that no putative adaptor protein is encoded in this cluster. To gain insights into the secretion mechanism of Tle1^{EAEC}, we tested direct pair-wise interactions between Tle1^{EAEC} and the *sci-1*-encoded Hcp1, VgrG1 and PAAR proteins by bacterial two-hybrid. Tle1^{EAEC} was fused downstream or upstream the T25 domain whereas the Hcp1, VgrG1 and PAAR proteins were fused to the T18 domain. The results presented in Fig. 7A indicate that Tle1^{EAEC} interacts directly with VgrG1, but not with Hcp1 or PAAR. The Tle1^{EAEC} -VgrG1

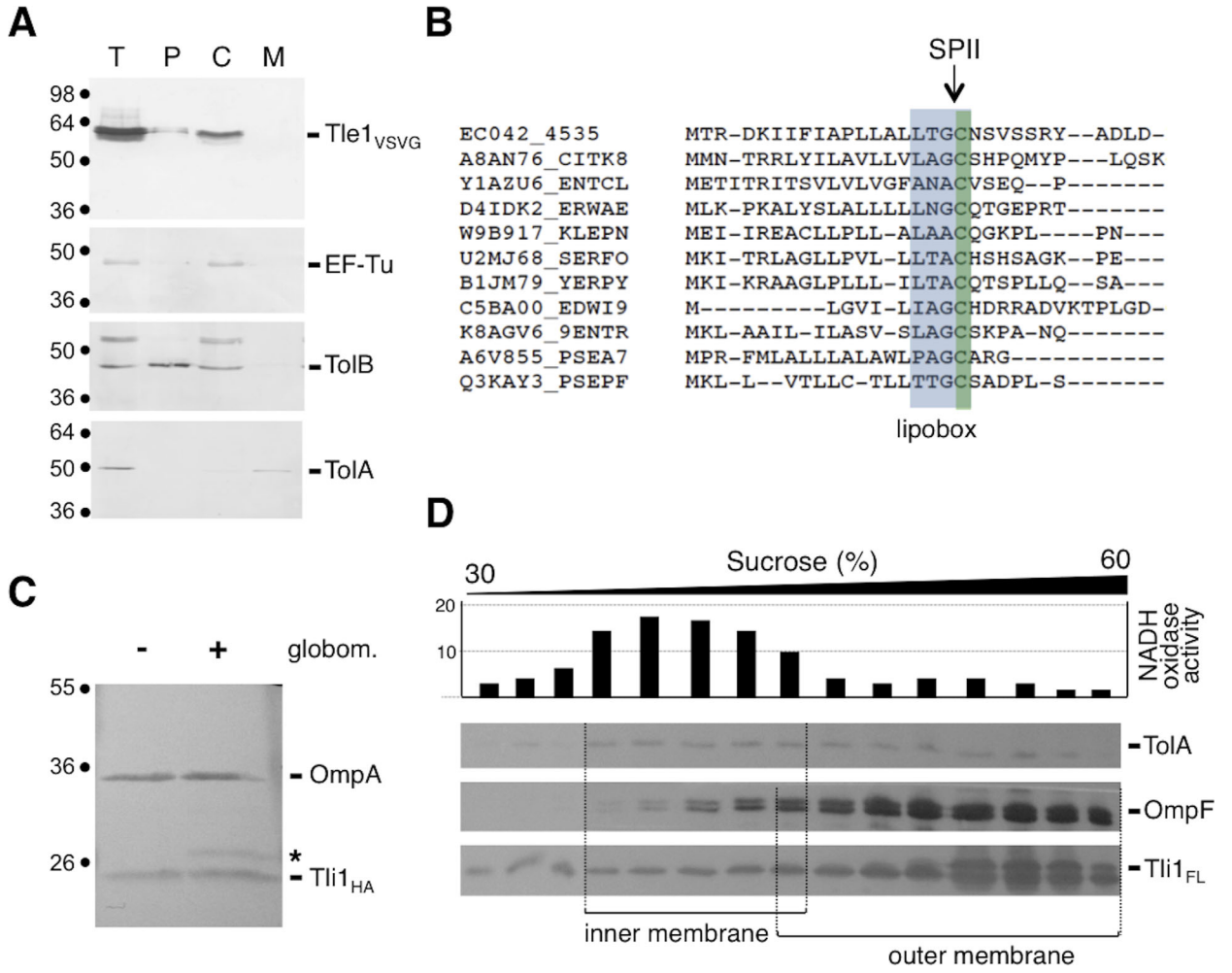

Fig. 5. Subcellular localizations of $Tle1^{EAEC}$ and $Tli1^{EAEC}$.
A. $Tle1^{EAEC}$ is a cytoplasmic protein. Total Δ*tle1-tli1* cells producing VSVG-tagged $Tle1^{EAEC}$ ($Tle1_{VSVG}$) (T) were fractionated to isolate the periplasmic (P), cytoplasmic (C) and membrane fractions (M). Proteins from 10^9 (T, M) and 2×10^9 (P, C) cells were separated by SDS-PAGE and immunodetected with anti-VSVG monoclonal ($Tle1_{VSVG}$), anti-EF-Tu (cytoplasmic marker), TolB (periplasmic marker) and TolA (membrane marker) antibodies. The position of the immunodetected proteins is indicated on the right. The molecular weight markers (in kDa) are indicated on the left.
B. $Tli1^{EAEC}$ bears a characteristic lipobox motif. ClustalW (T-Coffee) sequence alignment of the N-terminal region of the $Tli1^{EAEC}$ protein with that of representative homologous proteins (DUF2931 containing proteins) identified by HMMER analysis (Finn *et al.*, 2011). The putative lipobox motif (L-[G/A/S]-[G/A/S]-C) is indicated by a blue box. The position of the N-terminal cysteine residue of the processed form is underlined in green.
C. $Tli1^{EAEC}$ processing is dependent on signal peptidase II. EAEC Δ*tli1-tli1b* 2×10^9 cells producing HA-tagged $Tli1^{EAEC}$ ($Tli1_{HA}$) treated (+) or not (−) with the signal peptidase II inhibitor antibiotic globomycin were subjected to SDS-PAGE and immunodetection with the anti-HA and anti-OmpA antibodies. The unprocessed form of $Tli1_{HA}$ is indicated by an asterisk. The molecular weight markers (in kDa) are indicated on the left.
D. $Tli1^{EAEC}$ is an outer membrane protein. Total membrane from Δ*tli1-tli1b* cells producing FLAG-tagged $Tli1^{EAEC}$ ($Tli1_{FL}$) were separated on a discontinuous sedimentation sucrose gradient. The collected fractions were subjected to measurements of the NADH oxidase activity (inner membrane marker, represented as relative % to the total activity) (upper graph) and to SDS-PAGE and immunodetection with the anti-OmpF (outer membrane marker), anti-TolA (inner membrane marker) and anti-FLAG antibodies. The positions of outer and inner membrane fractions (based on control markers) are indicated.

interaction could not be detected with the T25-Tle1 fusion protein suggesting fusion to the N-terminus of $Tle1^{EAEC}$ may causes a steric hindrance preventing complex formation. To validate these data biochemically, we tested the VgrG1-$Tle1^{EAEC}$ interaction using a co-immunoprecipitation assay. To visualize direct interactions, the two proteins were produced into the *E. coli* K-12 heterologous host. Western-blot analyses of the eluted material showed that VSVG-tagged $Tle1^{EAEC}$ specifically co-immunoprecipitated with FLAG-tagged VgrG1, but not with $Hcp1_{FLAG}$ (Fig. 7B and Supporting Information Fig. S3). Taken together, the BACTH and

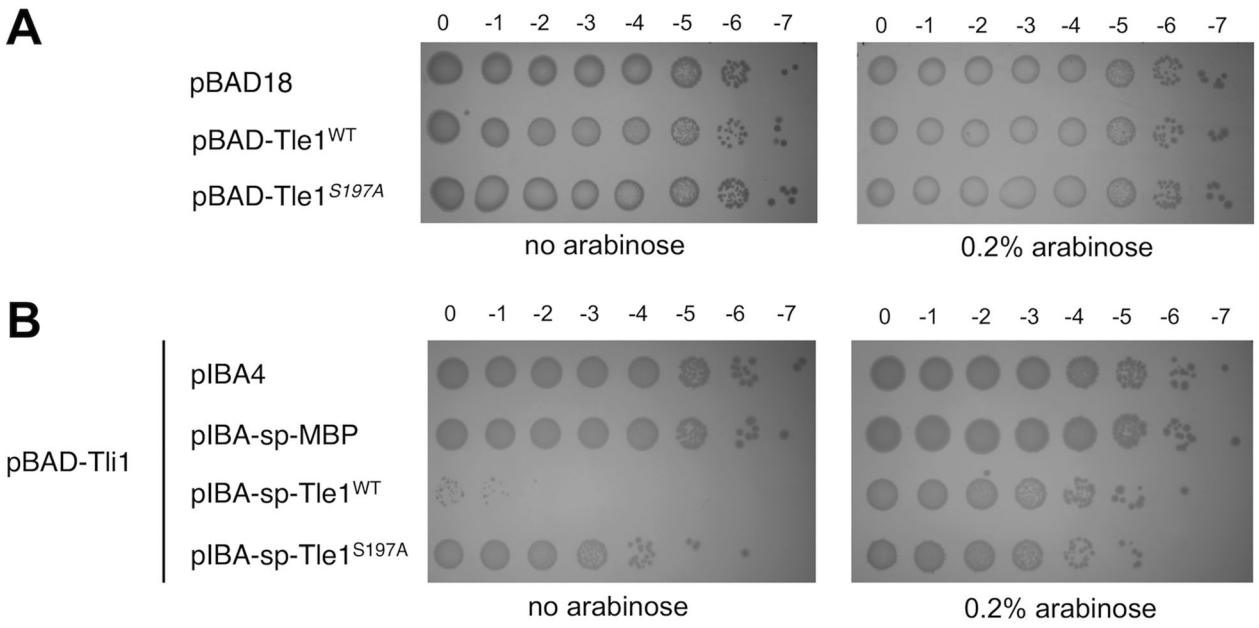

Fig. 6. Tle1^{EAEC} periplasmic toxicity is counteracted by Tli1^{EAEC}.
A. Cytoplasmic production of Tle1^{EAEC} is not toxic. Serial dilutions (from 0 to 10^{-7}) of normalized cultures of *E. coli* K-12 W3110 cells producing the WT (Tle1^{WT}) or the S197A mutant (Tle1^{S197A}) Tle1^{EAEC} proteins from the pBAD18 vector were spotted on LB agar plates supplemented (right panel) – or not (left panel) – with 0.2% arabinose.
B. Tli1^{EAEC} protects the cell against the toxicity of the periplasmic production of Tle1^{EAEC}. Serial dilutions (from 0 to 10^{-7}) of normalized cultures of *E. coli* K-12 W3110 cells producing Tli1^{EAEC} from the pBAD33 vector and the maltose-binding protein (MBP), the WT (Tle1^{WT}) or the S197A mutant (Tle1^{S197A}) proteins fused to a signal peptide (sp) from the pASK-IBA4 vector (periplasmic targeting) were spotted on LB agar plates supplemented (right panel) – or not (left panel) – with 0.2% arabinose.

co-immunoprecipitation assays demonstrate that Tle1^{EAEC} interacts with VgrG1.

Computer predictions and structural characterization of VgrG proteins showed that these proteins resemble the gp27-gp5 spike of bacteriophages (Pukatzki *et al.*, 2007; Leiman *et al.*, 2009). In EAEC, VgrG1 carries an additional C-terminal domain (CTD) separated from the gp27-gp5 common core by a predicted coiled-coil region (Fig. 7C). To assess the importance of this domain for the VgrG1-Tle1^{EAEC} interaction, we constructed VgrG truncated derivatives lacking this region (VgrG$_{1\text{-}615}$ lacking the CTD and VgrG$_{1\text{-}573}$ lacking both CTD and the predicted coiled-coil region). Co-immunoprecipitation and BACTH analyses showed that these truncations abolish Tle1^{EAEC} binding, suggesting that the VgrG1 CTD is necessary for the VgrG1-Tle1^{EAEC} interaction (Fig. 7B and D). Furthermore, this domain alone is sufficient to mediate the interaction with Tle1^{EAEC}, as shown by co-immunoprecipitation and BACTH experiments using the VgrG$_{574\text{-}841}$ and VgrG$_{616\text{-}841}$ derivatives (Fig. 7B and D). The VgrG1 CTD possesses a domain of unknown function of the DUF2345 family (amino-acid 609-765). DUF2345 domains are commonly found associated with T6SS VgrG proteins (Boyer *et al.*, 2009). Further bioinformatic analyses of this CTD using fold recognition servers such as Phyre2 and HHPred predicted that VgrG1 CTD amino-acid 611-766 region is constituted of a regular repetition of small short-strands that are reminiscent to the C-terminal domain of gp5 and likely extends the VgrG spike. This additional β-prism domain is followed by a 62-amino-acid region (residues 780–841) predicted to fold as a transthyretin (TTR)-like domain. To test the contribution of this domain to the VgrG1-Tle1^{EAEC} interaction, we constructed a VgrG1 truncated variant lacking the TTR-like region (VgrG$_{1\text{-}778}$). Figure 7D shows that VgrG$_{1\text{-}778}$ interaction with Tle1^{EAEC} is undetectable by BATCH analysis. However, VgrG$_{1\text{-}778}$ weakly interacts with Tle1^{EAEC} using the co-immunoprecipitation assay (Fig. 7B) suggesting that the absence of the TTR domain strongly affects but not completely abolishes the interaction with Tle1^{EAEC}. Further BACTH experiments suggest that this domain is sufficient to mediate the interaction with Tle1^{EAEC} as the VgrG$_{771\text{-}841}$/Tle1^{EAEC} combination activates the expression of the reporter gene (Fig. 7D). Attempts to confirm by co-immunoprecipitation that the TTR domain of VgrG1 is sufficient for this interaction was unsuccessful, as this truncated variant was undetectable by Western blot (data not shown). Collectively, these results show (i) that the VgrG1 CTD is necessary and sufficient for the

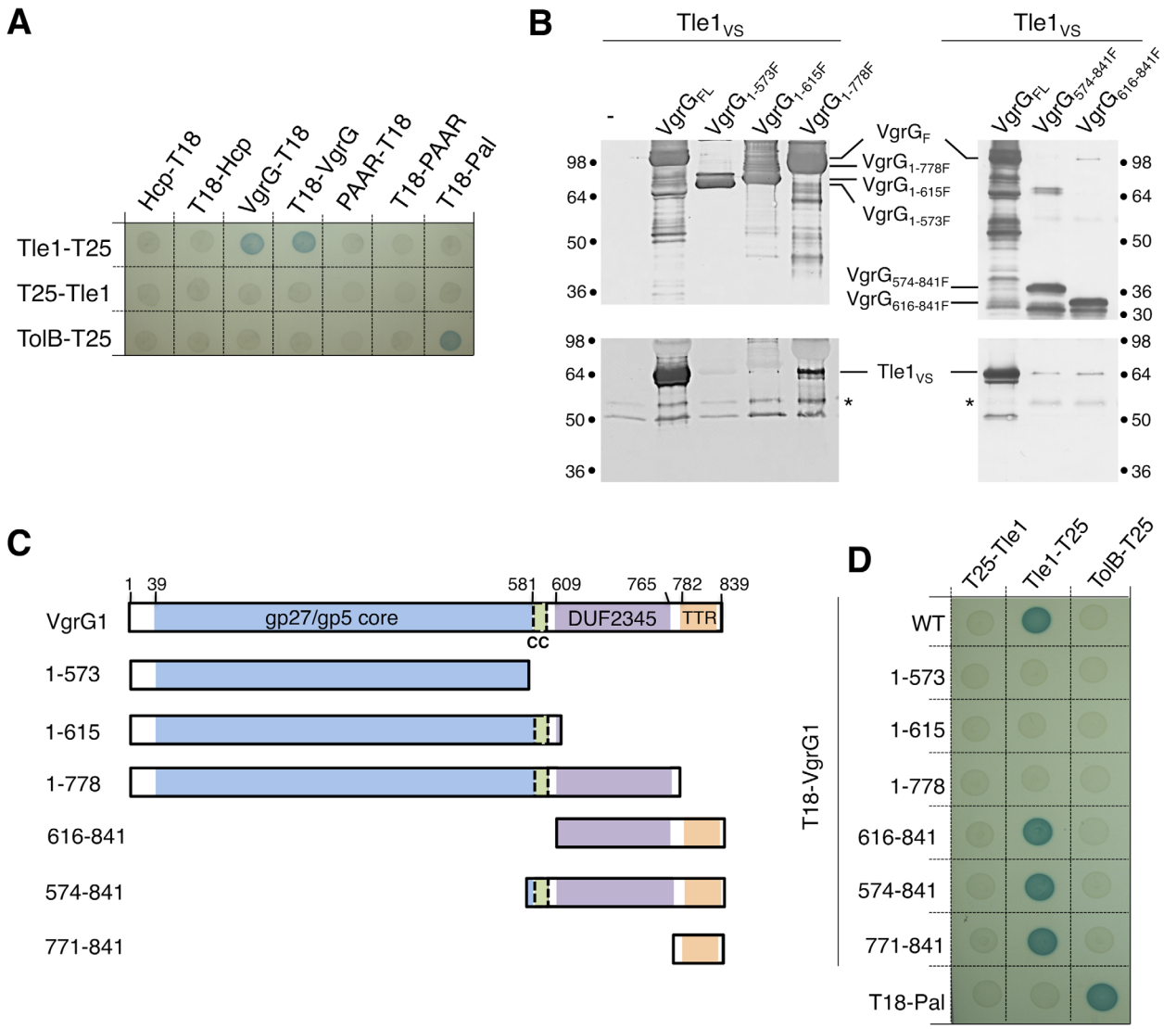

Fig. 7. Tle1^{EAEC} interacts with the VgrG1 C-terminal extension.
A. Tle1^{EAEC} interacts with VgrG, not with Hcp or PAAR. BTH101 reporter cells producing Tle1^{EAEC} fused to the T25 domain, and Hcp1, VgrG1 or PAAR proteins fused to the T18 domain of the *Bordetella* adenylate cyclase were spotted on X-Gal indicator plates. The blue colour of the colony reflects the interaction between the two proteins. Controls include T18 and T25 fusions to TolB and Pal, two proteins that interact but unrelated to the T6SS.
B. The CTD of VgrG1 is required and necessary for Tle1^{EAEC} co-immunoprecipitation. The soluble lysate from 10^{11} *E. coli* K-12 W3110 cells producing VSVG-tagged Tle1^{EAEC} (Tle1$_{VS}$) alone (-, empty vector) or mixed with soluble lysates of W3110 cells producing the FLAG-tagged full-length (VgrG$_F$) or variants of VgrG1 represented in panel (C) were immunoprecipitated on anti-FLAG-coupled beads. The immunoprecipitated material was subjected to 12.5%-acrylamide SDS-PAGE and immunodetected with anti-FLAG (upper panel) and anti-VSVG (lower panel) monoclonal antibodies. Molecular weight markers (in kDa) are indicated on the left. The asterisks indicate the position of the antibody heavy chain.
C. Schematic representation of the EAEC VgrG1 protein and of the truncated variants used in this study. The different domains (and their boundaries) are indicated (gp27 and gp5 structural core; cc, coiled-coil; DUF, DUF2345; TTR, transthyretin-like region).
D. The TTR C-terminal region of VgrG1 is necessary and sufficient for the interaction with Tle1^{EAEC}. BTH101 reporter cells producing Tle1^{EAEC} fused to the T25 domain, and the indicated VgrG1 fragments fused to the T18 domain of the *Bordetella* adenylate cyclase were spotted on X-Gal indicator plates. The blue colour of the colony reflects the interaction between the two proteins. Controls include T18 and T25 fusions to TolB and Pal, two proteins that interact but unrelated to the T6SS.

interaction with Tle1^{EAEC}, (ii) that the TTR domain of VgrG1 CTD is involved in the interaction but (iii) that a second interaction motif located within the 615-778 DUF2345 region stabilizes the VgrG1-Tle1 interaction.

To further test the importance of these interaction motifs for the delivery of Tle1^{EAEC}, we tested the ability of the VgrG1 C-terminal truncated derivatives to complement a *vgrG1* knock-out mutant in Hcp secretion and

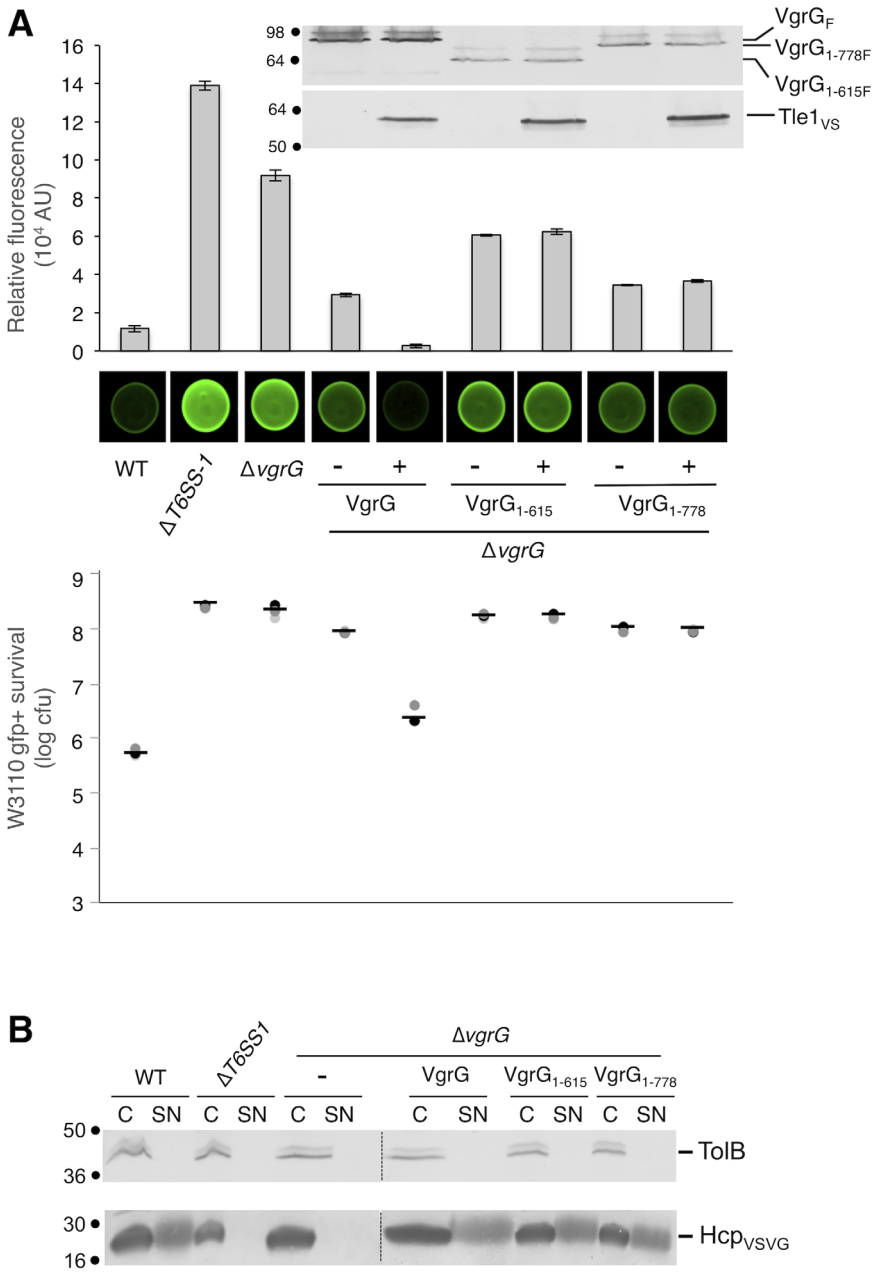

Fig. 8. The VgrG1 CTD is required for antibacterial activity but not for T6SS assembly.
A. The VgrG1 CTD is required for Tle1-dependent killing. The antibacterial activity was assessed by mixing W3110 *gfp*$^{+}$ prey cells with the indicated attacker cells: WT (EAEC 17-2), ΔT6SS-1 (*sci-1* gene cluster deletion derivative) and Δ*vgrG* (17-2 deleted of *vgrG1* gene) carrying the pBAD18 and pMS600 empty vectors, or producing the indicated proteins (Western-blot analyses shown in the inset), for 4 h at 37°C in *sci-1*-inducing medium containing 0.02% arabinose. The image of a representative bacterial spot is shown and the relative fluorescent levels (in AU) are indicated in the upper graph. The production of the VSV-G-tagged Tle1 protein and FLAG-tagged VgrG1 derivatives are shown in the inset. The number of recovered *E. coli* prey cells is indicated in the lower graph (in $\log_{10}$ of cfu). The circles indicate values from three independent assays, and the average is indicated by the bar.
B. The VgrG1 CTD is not required for proper assembly and function of the Sci-1 T6SS. Hcp release was assessed by separating whole cells (C) and supernatant (SN) fractions from WT (EAEC 17-2), Δ*T6SS-1* (*sci-1* gene cluster deletion derivative) and Δ*vgrG1* (17-2 deleted of *vgrG1* gene) carrying the pMS600 empty vector or producing the indicated VgrG1 variant, and pBAD-Hcp_{VSVG}. 0.5×10^9 total cells and the TCA-precipitated material from the supernatant of 10^9 cells were subjected to SDS-PAGE and immunodetection using anti-VSVG monoclonal antibody (lower panel) and anti-TolB polyclonal antibodies as a lysis control (upper panel). The molecular weight markers (in kDa) are indicated on the left.

killing assays (Fig. 8). The co-production of full length VgrG1 and Tle1 complemented the killing defect of the *vgrG* knock-out strain (Fig. 8A). By constrast, production of the truncated $VgrG_{1\text{-}615}$ or $VgrG_{1\text{-}778}$ variants (with or without the co-production of Tle1) did not restore killing (Fig. 8A). However, this result is not due to the assembly of a nonfunctional T6S apparatus as deletion of the VgrG1 CTD did not affect Hcp release (Fig. 8B). Taken together, these results showed that deletion of the Tle1-binding motif within VgrG1 does not impair T6SS assembly but abolishes killing of prey cells, hence supporting the idea that Tle1 interaction with the C-terminal extension of VgrG is required for Tle1 export into target cells.

Discussion

In this study, we show that the EAEC Sci-1 T6SS is required for interbacterial competition and report the full characterization of EC042_4534, the first T6SS toxin to be identified in EAEC, and EC042_4535, its cognate immunity protein. We demonstrate that EC042_4534 has phospholipase A activity, belongs to family 1 of the T6SS lipase effectors (Russell *et al.*, 2013), and was,

therefore, named Tle1^{EAEC}. A number of Tle proteins, delivered by the T6SS have been recently identified on the basis of their vicinity to *vgrG* genes. They consist of different enzymes divided into five divergent families (Russell *et al*., 2013). Tle families 1–4 contain a characteristic GXSXG esterase motif found in lipases and some phospholipases. *In vitro* studies have shown that the *Burkholderia thailandensis* Tle1^{BT} and *P. aeruginosa* Tle1^{PA} effectors have PLA_2 activity (Russell *et al*., 2013; Hu *et al*., 2014). By contrast, the *Vibrio cholerae* Tle2^{VC} toxin carries PLA_1 activity (Russell *et al*., 2013). No enzymatic activity has been assigned so far for members of the Tle3 and Tle4 families. Tle5 family members contain a duplicated HXDXXXXG motif characteristic of phospholipase D (PLD) superfamily, and can be divided in two subfamilies (Tle5a and Tle5b), with Tle5a being eukaryotic-like PLD (Russell *et al*., 2013; Jiang *et al*., 2014; Egan *et al*., 2015; Spencer and Brown, 2015). The PLD activities of *P. aeruginosa* Tle5a^{PA} (known as PldA) and Tle5b^{PA} (known as PldB) have been demonstrated (Russell *et al*., 2013; Jiang *et al*., 2014; Spencer and Brown, 2015), while *Klebsiella pneumoniae* Tle5b^{KP} T6SS toxin presents a cardiolipin synthase activity (Lery *et al*., 2014).

Our analyses showed that Tle1^{EAEC} has PLA_1 and to a lesser extent PLA_2 activity, which contrasts with the previously characterized Tle1 members, Tle1^{BT} and Tle1^{PA}, which have PLA_2 activity only (Russell *et al*., 2013; Hu *et al*., 2014). It is noteworthy that the Tle classification was built on their protein sequences and phylogenetic distribution, and not on their activity. It remains possible that Tle1 members may not have all the same selectivity for the sn-1 and sn-2 positions. Tle1 toxins consist to very heterologous proteins in terms of size ($\sim$ 500–900 residues). They all possess a DUF2235 (α/β hydrolase fold domain) likely forming the catalytic module but bear distinct additional domains. For example, Tle1^{PA} has a putative C-terminal membrane-anchoring module (Hu *et al*., 2014) that has been shown to be critical for the catalytic activity, suggesting that the activity of Tle1 proteins might also be regulated by these additional domains. Further biochemical and structural characterizations of Tle1^{EAEC} and other Tle1 proteins are, therefore, required to better understand the differences in substrate selectivity on the phospholipid sn-1 and sn-2 moieties.

Our results also showed that Tle1^{EAEC} is required for the antibacterial activity conferred by the Sci-1 T6SS. Tle1^{BT} and Tle4^{APEC} were previously shown to be required for the antibacterial activity of *B. thailandensis* and avian pathogenic *E. coli* respectively (Russell *et al*., 2013; Ma *et al*., 2014). By contrast, Tle5a^{PA} (PldA) and Tle5b^{PA} (PldB) are required for both bacterial competition and virulence (Jiang *et al*., 2014). Tle5b^{PA} delivery into eukaryotic host cells promotes invasion through the activation of the AKT/PI3pathway (Jiang *et al*., 2014). Similarly, the Tle2^{VC} toxin is necessary for the antibacterial activity of *V. cholerae* and its ability to escape amoeba predation (Dong *et al*., 2013). In *K. pneumoniae*, Tle5^{KP} is required for full virulence in a mouse model of infection (Lery *et al*., 2014). Although we did not observe any effect of the Sci-1 T6SS on *C. elegans* viability, we cannot rule out that the Tle1^{EAEC} toxin might be delivered into eukaryotic host cells to create damages. It would be interesting to test the role of the Sci-1 T6SS and of its specific Tle1^{EAEC} toxin on epithelial intestinal cells.

Our results also demonstrated that the production of Tle1^{EAEC} in the cytoplasm of *E. coli* K-12 has no effect on its viability. By contrast, cells do not survive when Tle1^{EAEC} is exported to the periplasm. This result is consistent with the observations that the heterologous periplasmic production of Tle1^{PA}, Tle5a^{PA} and Tle5b^{PA} is toxic (Jiang *et al*., 2014; Hu *et al*., 2014). One may hypothesize that (i) Tle1^{EAEC} targets specific lipids found in the outer leaflet of the inner membrane or in the inner leaflet of the outer membrane and/or (ii) that dedicated periplasmic proteins are required to activate Tle1^{EAEC}, as previously shown for the colicin M toxin (Hullmann *et al*., 2008). The activity of Tle toxins in the periplasm is in agreement with the synthesis of a cognate immunity protein called Tli that are usually periplasmic soluble proteins or membrane-anchored lipoprotein (Russell *et al*., 2013). In this work, we have shown that Tli1^{EAEC} (EC042_4535) confers protection against Tle1^{EAEC}. Fractionation, isopycnic centrifugation and processing inhibition assays demonstrated that Tli1^{EAEC} is an outer membrane lipoprotein. Tli1^{EAEC}-mediated inhibition of Tle1^{EAEC} occurs by protein–protein contacts and is very efficient, as a molecular ratio of 1:1 totally abolishes Tle1^{EAEC} phospholipase activity. The interaction between the two partners was observed *in vivo* by bacterial two-hybrid analyses and biochemical approaches. Other immunities to phospholipases characterized so far have been shown to inhibit the action of the effector by direct protein–protein contacts, such as the *P. aeruginosa* Tle5/Tli5 pairs (Russell *et al*., 2013; Jiang *et al*., 2014). *In vitro* analyses of the purified Tle1^{EAEC}/Tli1^{EAEC} complex by gel filtration, MALS/QELS/UV/RI and BLI collectively demonstrated that Tle1^{EAEC} interacts with Tli1^{EAEC} with a 1:1 stoichiometry and a K_D of 1.5 nM. This tight binding, with a very fast association and a very slow dissociation is in accordance with the role of Tli1^{EAEC} as a specific immunity protein, as the control of Tle1^{EAEC} activity should be strict among bacteria from the same species and should occur rapidly after delivery of Tle1^{EAEC}. This nanomolar affinity is in the same range as other T6SS effector/immunity pairs such as Tae1/Tai1 couples (Ding *et al*., 2012; Shang *et al*., 2012) and suggests an extensive surface of contact

between the two partners. Indeed, the crystal structure of the putative *P. aeruginosa* Tle4 effector in complex with its putative immunity protein (Tli4^{PA}) revealed that Tli4^{PA} covers a surface area of $\sim$ 2800 Å^2 and use a grasp mechanism to prevent the interfacial activation of Tle4^{PA} (Lu *et al*., 2014). Further structural characterization of the EAEC Tle1/Tli1 complex is required to better understand the molecular bases for this efficient inhibition.

In this work, we also addressed the secretion mechanism of Tle1^{EAEC}. Several mechanisms have been identified or proposed for independent effectors, and all of them involve direct or indirect contacts with the Hcp rings, the VgrG spike or the PAAR protein that sits on VgrG (Shneider *et al*., 2013; Silverman *et al*., 2013; Durand *et al*., 2014; Hachani *et al*., 2014; Whitney *et al*., 2014). Recently, conserved adaptor proteins of the DUF4123 family interacting with both VgrG and the effector were shown to be required for the translocation of a number of T6SS effectors (Liang *et al*., 2015; Unterweger *et al*., 2015). Here, co-immunoprecipitation and bacterial two-hybrid analyses demonstrated that Tle1^{EAEC} interacts directly with VgrG1 and that this interaction is required for proper Tle1^{EAEC} delivery. A gene encoding a putative PAAR protein, *EC042_4537*, is found immediately downstream Tli1. However, PAAR is not required for the VgrG1/Tle1^{EAEC} direct interaction, suggesting that it constitutes a structural element at the tip of the VgrG spike or that it is involved in the recruitment and transport of a yet unidentified effector. In the cargo transport hypothesis, the VgrG proteins are used as carriers to deliver effectors into the target cell (Durand *et al*., 2014). In *P. aeruginosa*, several toxins have been shown to be dependent on dedicated VgrG proteins for their delivery suggesting that VgrG proteins bear specific sequences to select cognate effectors (Hachani *et al*., 2014; Whitney *et al*., 2014). Our results support this idea as we found that the C-terminal extension of VgrG1 is necessary and sufficient to mediate binding to and transport of Tle1^{EAEC}. Particularly, we identified a region of 62 amino-acids at the C-terminus of VgrG1 involved in this interaction. This short domain is predicted to fold as a transthyretin-like (TTR) domain. TTR domains are putative protein–protein interaction modules. Interestingly, TTR domains were previously identified as PAAR protein extensions, and were proposed to be adaptors to mediate interaction with effector proteins (Shneider *et al*., 2013). However, deletion of the TTR domain of VgrG1 did not totally abolish the interaction with Tle1^{EAEC}, suggesting that another motif may be present in the DUF2345 domain of VgrG1. Collectively, these results demonstrate that DUF2345/TTR domains are involved in selection and transport of T6SS effectors. One may hypothesize that distinct motifs should be involved in the recruitment of effectors to confer specificity. Indeed, although this needs to be experimentally verified, a disordered loop within the C-terminal β-helix of the *E. coli* O157 VgrG1 protein was proposed to be an interaction site with effectors (Uchida *et al*., 2014). Similarly, the recent release of the structure of the *P. aeruginosa* VgrG1 spike (PDB: 4UHV; Spinola-Amilibia *et al*., 2016) reveals the existence of a small C-terminal helix that folds along the VgrG β-helix. We, therefore, propose that additional CTDs in VgrG and likely on PAAR proteins might be considered as internal adaptors for interaction with effectors and that the EAEC VgrG1 DUF2345/TTR domain represents such a motif. Further experiments on different T6SS effectors will likely highlight the diversity of these selection modules.

Experimental procedures

Bacterial strains, growth conditions and chemicals

The *E. coli* strains and plasmids used in this study are listed in Supporting Information Table S1. The enteroaggregative *E. coli* EAEC strain 17-2 and its Δ*T6SS-1*, Δ*tle1-tli1*, Δ*tli1-tli1b* isogenic derivatives were used for this study. *Escherichia coli* K-12 DH5α, W3110, BTH101 and T7-Iq pLys strains were used for cloning steps, co-immunoprecipitation, bacterial two-hybrid and protein purification respectively. The *E. coli* K-12 W3110 strain carrying the pUA66-*rrnB* plasmid [*gfp* under the control of the constitutive *rrnB* ribosomal promoter, specifying strong and constitutive fluorescence, and kanamycin resistance (Zaslaver *et al*., 2006)] was used as prey in antibacterial competition experiments. Strains were routinely grown in LB rich medium (or Terrific broth medium for protein purification) or in *sci-1* inducing medium (SIM; M9 minimal medium, glycerol 0.2%, vitamin B1 1 μg/ml, casaminoacids 100 μg/ml, LB 10%, supplemented or not with bactoagar 1.5%) with shaking at 37°C. Nematode growth plates (NGM) were used for the *C. elegans* infection assay. Plasmids were maintained by the addition of ampicillin (100 μg/ml for *E. coli* K-12, 200 μg/ml for EAEC), kanamycin (50 μg/ml) or chloramphenicol (30 μg/ml). Expression of genes from pBAD, pOK12 and pASK-IBA vectors was induced at exponential phase for 1 h with 0.1% of L-arabinose (Sigma-Aldrich), 100 μM of isopropyl-D-thio-galactopyrannoside (IPTG, Eurobio) and 0.1 μg/ml of anhydrotetracyclin (AHT, IBA Technologies) respectively. 5-Bromo-4-chloro-3-indolylβ-D-galactopyranoside (X-Gal, Eurobio) was used at 40 μg/ml. Globomycin (a kind gift of Dr. Danièle Cavard) was used at 50 μg/ml. Oligonucleotides and plasmids used in this study are listed in Supporting Information Table S1.

Strain construction

The *tle1 (EC042_4534) and tli1 (EC042_4535)* genes were deleted into the EAEC 17-2 WT strain using a modified one-step inactivation procedure (Datsenko and Wanner, 2000) as previously described (Aschtgen *et al*., 2008) using

oligonucleotide pairs DEL-4534-5-DW/DEL-4534-3-DW. This oligonucleotide pairs carry 50-nucleotide 5′ extensions homologous to regions adjacent to *tle1*. Because *tli1* is duplicated (*tli1b* has the same 5′ sequence than *tli1*), attempts to delete *tle1* only yielded to the deletion of both *tle1* and *tli1* genes (Δ*tle1-tli1*). The *tli1 (EC042_4535)* and *tli1b (EC042_4536)* genes were deleted into 17-2 WT strain as described above using oligonucleotide pairs DEL-4535-5-DW/DEL-4535-3-DW. Kanamycin resistant clones were selected and verified by colony-PCR. The kanamycin cassette was then excised using plasmid pCP20. The deletions of the gene of interest were confirmed by colony-PCR and complementation studies.

Plasmid construction

Custom oligonucleotides were synthesized by Sigma Aldrich and are listed in Supporting Information Table S1. EAEC *E. coli* 17-2 chromosomal DNA was used as a template for all PCRs. *Escherichia coli* strain DH5 was used for cloning procedures. Polymerase chain reactions (PCR) were performed using a Biometra thermocycler using the Q5 High fidelity DNA polymerase (New England Biolabs). All the plasmids (except pETG20A and pOK12 derivatives) have been constructed by restriction-free cloning (van den Ent and Löwe, 2006) as previously described (Aschtgen *et al*., 2010a). Briefly, genes of interest were amplified with oligonucleotides introducing extensions annealing to the target vector. The double-stranded product of the first PCR has then been used as oligonucleotides for a second PCR using the target vector as template. For the pETG20A-Tle1 and pETG20A-Tli1 constructs, the genes encoding $Tle1^{EAEC}$ and signal sequence-less $Tli1^{EAEC}$ were amplified by PCR using specific Gateway® primers containing *attB* sequences, which allow insertion into the pDONR201 cloning vector by the BP recombination reaction, and then introduced into the pETG20A vector. The final constructs allow the production of $Tle1^{EAEC}$ or $Tli1^{EAEC}$ fused to an N-terminal hexahistidine-tagged thioredoxin (TRX) followed by a TEV protease cleavage site. For pOK-Tli_{HA}, pOK-$VgrG_F$, pOK-$VgrG_{1\text{-}573F}$ and pOK-$VgrG_{1\text{-}615F}$, the coding sequence of *tli*, *vgrG* and the different *vgrG* domains were amplified by PCR using oligonucleotides introducing *Eco*RI and *Xho*I restriction sites and cloned into the pOK12-derivative vector pMS600 (Aschtgen *et al*., 2008) digested by the same enzymes. In addition, the 3' oligonucleotide contains the sequence encoding the FLAG epitope, allowing C-terminal in-frame fusion of the *vgrG* derivatives with the FLAG epitope. The Ser197-to-Ala substitution was introduced in the pETG20A-Tle1, pBAD-Tle1-Tli1 and the pIBA-sp-Tle1 plasmids by QuickChange PCR-based targeted mutagenesis (Supporting Information Table S1). Mutations were confirmed by DNA sequencing (GATC Biotech or Eurofins).

Caenorhabditis elegans *infection assay*

Virulence towards *C. elegans* was tested by a slow killing assay. L4 to adult stage nematods grown on *E. coli* OP50 were placed on unseeded NGM plates for 24 h at 25°C. Twenty-five worms were then picked and placed onto lawns of bacteria to be tested. The viability of each individual was evaluated on a daily basis and the number of surviving nematods was plotted over time. The *E. coli* K-12 OP50 and *B. cenocepacia* K56-2 strains have been used as controls.

Interbacterial competition assay

The antibacterial growth competition assay was performed as described for the studies on the *Citrobacter rodentium* and EAEC Sci-2 T6SSs (Brunet *et al*., 2013; Gueguen and Cascales, 2013) with modifications. The WT *E. coli* strain W3110 bearing the pUA66-*rrnB* plasmid [Kan^R (Zaslaver *et al*., 2006)] was used as prey in the competition assay. The pUA66-*rrnB* plasmid provides a strong constitutive green fluorescent (GFP^+) phenotype. Attacker and prey cells were grown for 16 h in SIM medium, and then diluted in SIM to allow maximal expression of the *sci-1* gene cluster (Brunet *et al*., 2011). Once the culture reached an $OD_{600nm} \sim 0.8$, cells were harvested and normalized to an OD_{600nm} of 10 in SIM. Attacker and prey cells were mixed to a 4:1 ratio and 20-μl drops of the mixture were spotted in triplicate onto a prewarmed dry SIM agar plate supplemented or not with arabinose 0.02% or IPTG 20 μM. After 4-hour incubation of the plates at 37°C, fluorescent images were recorded with a LI-COR Odyssey imager. The bacterial spots were scratched off, and cells were resuspended in LB medium supplemented with chloramphenicol and normalized to an OD_{600nm} of 0.5. Triplicates of 200 μl were transferred into wells of a black 96-well plate (Greiner) and the absorbance at 600 nm and fluorescence (excitation, 485 nm; emission, 530 nm) were measured with a Tecan Infinite M200 microplate reader. The relative fluorescence was expressed as the intensity of fluorescence divided by the absorbance at 600 nm, after subtracting the values of a blank sample. These results are given in arbitrary units (AU) because the intensity of fluorescence is acquired with a variable gain and hence varies from one experiment to the other. For estimation of cfu, fluorescent Kan^R colonies were enumerated under UV light. The experiments were done in triplicate, with identical results, and we report here the results of a representative experiment.

Computer algorithms for phylogenetic analyses and $Tle1^{EAEC}$ structure modelling

Phylogenetic tree reconstruction has been made using Phylogeny.fr (Dereeper *et al*., 2008). The homology model of $Tle1^{EAEC}$ was built with C*oot* (Emsley *et al*., 2010) based on a Multalin alignment with the published *P. aeruginosa* effector $Tle1^{PA}$ (PDB: 4O5P, Hu *et al*., 2014). The regions present in $Tle1^{EAEC}$ but not in 4O5P were not included in the modelling.

Bacterial two-hybrid assay

The adenylate cyclase-based bacterial two-hybrid technique (Karimova *et al*., 1998) was used as previously published (Battesti and Bouveret, 2012). Briefly, pairs of proteins to be tested were fused to the isolated T18 and T25 catalytic domains of the *Bordetella* adenylate cyclase. After

transformation of the two plasmids producing the fusion proteins into the reporter BTH101 strain, plates were incubated at 30°C for 48 h. Three independent colonies for each transformation were inoculated into 600 μl of LB medium supplemented with ampicillin, kanamycin and IPTG (0.5 mM). After overnight growth at 30°C, 10 μl of each culture were dropped onto LB plates supplemented with ampicillin, kanamycin, IPTG and X-Gal and incubated for 16 h at 30°C. The experiments were done at least in triplicate and a representative result is shown.

Purification of Tle1, Tle1^{S197A} and Tli1

Escherichia coli T7 Iq pLys cells carrying the pETG20A-Tle1, pETG20A-Tle1^{S197A} or pETG20A-Tli1 plasmids were grown at 37°C in terrific broth to an $OD_{600} \sim 0.9$ and *tle1, tle1*^{S197A} or *tli1* expression was induced with IPTG (0.5 mM) for 16 h at 17°C. Cells were harvested by centrifugation and stored at −80°C. The cell pellet was resuspended in Tris-HCl 20 mM pH 8.0, NaCl 300 mM, glycerol 5% (v/v), lysozyme (0.25 mg/ml), DNase (2 μg/ml), $MgSO_4$ 20 mM and phenylmethylsulfonyl fluoride 1 mM and cells were lysed by ultrasonication on ice. The insoluble material was discarded by centrifugation at 20,000 *g* for 60 min at 4°C. The soluble thioredoxin 6× His-tagged Tle1, Tle1^{S197A} or Tli1 fusion proteins were purified by affinity chromatography on a nickel–nitrilotriacetic acid resin (Bio-Rad) and the tag was removed after dialysis by overnight hydrolysis with the TEV protease and reloading in presence of 10 mM imidazole. The proteins were further purified by gel filtration chromatography (Superdex 75, 10/30 GE Healthcare) equilibrated in Tris-HCl 20 mM pH 8.0, NaCl 300 mM, dithiothreitol (DTT) 2 mM using an AKTA purifier System (Amersham). The purified protein fractions were pooled and concentrated to ∼ 15 mg/ml by ultrafiltration using the Amicon technology (Millipore, California, USA). For phopholipase activity assays, the purified Tle1 and Tle1^{S197A} proteins were concentrated to 0.6 mg/ml.

Purification of the Tle1^{EAEC}-Tli1^{EAEC} complex

Purified Tle1^{EAEC} and Tli ^{EAEC} were mixed together in a molar ratio of 1:1.2. The complex was purified by gel filtration chromatography (Superdex 75, 10/30 GE Healthcare) equilibrated in a Tris-HCl 20 mM pH 8.0, NaCl 150 mM buffer using an AKTA purifier System (Amersham). The fractions containing the complex were pooled and concentrated to ∼ 15 mg/ml as described above.

MALS/QELS/UV/RI-coupled size exclusion chromatography

Size exclusion chromatography was performed on an Alliance 2695 HPLC system (Waters) using a precalibrated KW802.5 column (Shodex) run in HEPES 25 mM pH 7.3, NaCl 250 mM at 0.5 ml/min. MALS, UV spectrophotometry, QELS and RI were achieved with MiniDawn Treos (Wyatt Technology), a Photo Diode Array 2996 (Waters), a DynaPro (Wyatt Technology) and an Optilab rEX (Wyatt Technology), respectively, as described (Sciara *et al.*, 2008). Mass and hydrodynamic radius calculation was done with ASTRA software (Wyatt Technology) using a *dn*/*dc* value of 0.185 ml/g.

Biolayer interferometry

The purified Tli1^{EAEC} protein was first biotinylated using the EZ-Link NHS-PEG4-Biotin kit (Perbio Science, France). The reaction was stopped by removing the excess of biotin using a Zeba Spin Desalting column (Perbio Science, France). BLI studies were performed in black 96-well plates (Greiner) at 25°C using an OctetRed96 (ForteBio, USA). Streptavidin biosensor tips (ForteBio, USA) were first hydrated with 0.2 ml Kinetic Buffer (KB, ForteBio, USA) for 20 min and then loaded with biotinylated Tli1^{EAEC} (10 g/ml in KB). The association of Tli1^{EAEC} with various concentrations of Tle1 (0.4 nM, 1 nM, 2.56 nM, 6.4 nM, 16 nM and 40 nM) was monitored for 600 s, and the dissociation was followed for 1800 s in KB.

Phospholipase A1 and A2 fluorescent assays

Phospholipase activities of Tle1^{EAEC} and Tle1^{S197A} were performed using fluorogenic phospholipid substrates. Phospholipase A_1 and A_2 activities were monitored continuously using BODIPY® dye-labeled phospholipids: PED-A_1 (N-((6-(2,4-DNP)Amino)Hexanoyl)−1-(BODIPY® FL C5)−2-Hexyl-*sn*-Glycero-3-Phosphoethanolamine**)** and red/green BODIPY® PC-A_2 (1-O-(6-BODIPY-®558/568-Aminohexyl)−2-BODIPY®FLC5-*sn*-Glycero-3-Phosphocholine) respectively (Farber *et al.*, 2001; Darrow *et al.*, 2011). The *sn*−2 fatty acyl group in PED-A_1 is a non-hydrolyzable alkyl chain, and PED-A_1 substrate was used to specifically measure the PLA_1 activity. The red/green BODIPY® PC-A_2 has a *sn*−1 uncleavable alkyl chain. Substrate stock solutions (50 μM) were prepared in ethanol. All enzyme activities were assayed in Tris-HCl 10 mM pH 8.0, NaCl 150 mM, $CaCl_2$ 1 mM and Triton X-100 0.1%. Enzymatic reactions were performed at 20°C for 25 min in a final volume of 200 μl containing 20 μg of Tle1 purified protein (from a 0.6 mg ml^{-1} stock solution) and 5 μM of the substrate. During pilot studies, we noted that concentrations of the purified Tle1 protein above 1 mg ml^{-1} led to a decrease in the measured Tle1 PLA_1 specific activity. The release of BODIPY® (BFCL5) (Life Technologies) was recorded at $\lambda_{exc} = 485$ nm and $\lambda_{em} = 538$ nm using a 96-well plate fluorometer (Fluoroskan ascent, Thermoscientific). Enzymatic activities were quantified using a BFCL5 calibration curve (0.08–200 pmoles in activity buffers) and expressed in pmol of fatty acid (or BFLC5) released per minute per mg of protein (pmol min^{-1} mg^{-1}). PLA_1 from *Thermomyces lanuginosus* and Bee venom PLA_2 (Sigma-Aldrich, Saint-Quentin Fallavier, France) were used as positive standards for PLA_1 and PLA_2 activities respectively. Inhibition studies with Tli1^{EAEC} were performed by incubating 20 μg of Tle1^{EAEC} with various molar ratio of Tli1^{EAEC} ($x_i = 0.125$, 0.25, 0.5, 1 and 2). The residual activity was measured as described above.

Activities on phospholipid monolayer films

All experiments were performed using the KSV5000 system (KSV, Helsinki, Finland) equipped with a Langmuir film

balance to measure the surface pressure (Π) and monitored by the KSV Device Server Software v.3.50 running under Windows 7® as previously described (Point *et al.*, 2013). A Teflon 'zero-order' trough (Verger and de Haas, 1973) was filled with Tris-HCl 10 mM pH 8.0, NaCl 100 mM, $CaCl_2$ 21 mM and EDTA 1 mM. The phospholipid monolayer was formed at the desired surface pressure (Π) of 20 mN m^{-1} by spreading a few microliters of a phospholipid solution (1 mg/ml in chloroform containing 0.4% v/v methanol) and further incubation for $>$ 10 min (chloroform evaporation). Hydrolysis rate measurements were performed with a Teflon 'zero-order' trough with two compartments: a reaction compartment (volume 43 ml; surface area, 38.5 cm^2) and a reservoir compartment (volume 203 ml; surface area, 156.5 cm^2) connected to each other by a small surface channel. The purified $Tle1^{EAEC}$ protein was injected into the subphase of the reaction compartment only (11 nM enzyme final concentration), whereas the phospholipid lipid film spread at the air–water interface covers both of them. When using medium chain phospholipids, such as DLPC, DLPG, DLPS or DLPE, soluble lipolysis products are released upon the action of phospholipase and a drop in surface pressure can be recorded. Using the barostat mode available on the KSV5000 instrument, an automatically driven Teflon mobile barrier can be moved over the reservoir to compress the phospholipid film and compensate for the substrate molecules removed from the film by the enzyme hydrolysis, thus keeping the surface pressure constant (here at $\Pi = 20$ mN m^{-1}). The kinetics of hydrolysis were recorded for at least 60 min and PLA activities (mol cm^{-2} min^{-1} M^{-1}) were expressed as the number of moles of substrate hydrolyzed per time unit (min) and per surface unit (cm^2) of the reaction compartment of the 'zero-order' trough and for an arbitrary enzyme concentration of 1 M (de la Fournière *et al.*, 1994).

Globomycin treatment

EAEC cells producing HA-tagged Tli1 from pOK-$Tli1_{HA}$ were grown to an optical density at 600 nm (OD_{600}) of ~0.6 prior to the addition of 50 μg/ml of globomycin. After 10 min of treatment, IPTG was then added at a final concentration of 100 μM, and cells were further incubated for 30 min at 37°C. Cells were harvested, and samples were analyzed by sodium dodecyl sulfate (SDS)-polyacrylamide gel electrophoresis (PAGE) and immunoblotting.

Escherichia coli *K-12 toxicity assays*

Cells were grown in LB at 37°C for 16 h. Bacterial suspensions were normalized to an OD_{600} of 2, serially diluted and 15 μl drops of each dilution were spotted onto selective LB agar plates containing or not arabinose 0.2%.

Co-immunoprecipitation experiments

One hundred millilitre of W3110 cells producing the proteins of interest from independent plasmids were grown to and OD_{600} ~ 0.4 and the expression of the cloned genes was induced with IPTG 200 μM or arabinose 0.2% for 1 h. The cells were harvested and the pellets were frozen in liquid nitrogen and stored at −80°C for 1 h. Pellets were then resuspended in Tris-HCl 20 mM pH 8.0, NaCl 100 mM, sucrose 30%, lysozyme 100 μg/ml, EDTA 1 mM, DNase 100 μg/ml, RNase 100 μg/ml, Complete protease inhibitor cocktail (Roche) to an OD_{600} ~ 100 and incubated on ice for 15 min. An equal volume of Tris-HCl 20 mM pH 8.0, NaCl 100 mM, $MgCl_2$ 5 mM was then added, and the cells were lysed by two passages at the French Press (800 psi). Lysates were clarified by centrifugation at 13,000 *g* for 10 min. Supernatants were used for co-immunoprecipitation using Anti-FLAG® M2 affinity gel (Sigma-Aldrich). After 3 h of incubation, the beads were washed twice with 1 ml of Tris-HCl 20 mM pH 8.0, NaCl 100 mM, sucrose 15%, and once with Tris-HCl 20 mM pH 8.0, NaCl 100 mM. Beads were recovered and resuspended in 25 μl of SDS-loading buffer and heated for 10 min at 96°C prior to SDS-PAGE and Western-blot analyses.

Miscellaneous

Fractionation, sedimentation sucrose gradient assays, NADH oxidase activity measurements and Hcp release assay have been performed as previously described (Aschtgen *et al.*, 2008; Aschtgen *et al.*, 2010). SDS-Polyacrylamide gel electrophoresis was performed using standard protocols. For immunostaining, proteins were transferred onto 0.2 μm nitrocellulose membranes (Amersham Protran), and immunoblots were probed with primary antibodies (see below) and goat secondary antibodies coupled to alkaline phosphatase and developed in alkaline buffer in presence of 5-bromo-4-chloro-3-indolylphosphate and nitroblue tetrazolium. The anti-TolB, anti-TolA, anti-OmpA and anti-OmpF polyclonal antibodies are from our laboratory collection, while the anti-HA (3F10 clone, Roche), anti-FLAG (M2 clone, Sigma Aldrich), anti-EF-Tu (Roche) and anti-VSVG (Sigma-Aldrich) monoclonal antibodies and alkaline phosphatase-conjugated goat anti-rabbit, mouse or rat secondary antibodies (Millipore) have been purchased as indicated.

Acknowledgements

We thank Jean-François Cavalier for phospholipid monolayer film experiments, Danièle Cavard for providing globomycin, Steve Garvis for help with the *Caenorhabditis elegans* model, Abir Benzeggouta for initial Tli1 constructs and Anant Kumar for constructing the pBAD-Hcp_{VSVG}. We thank Emmanuelle Bouveret, James Sturgis, Abdelrahim Zoued and the members of the Cascales, Lloubès, Bouveret and Sturgis research groups for insightful discussions, Annick Brun, Isabelle Bringer and Olivier Uderso for technical assistance. Work in E.C. laboratory is supported by the Centre National de la Recherche Scientifique (CNRS), the Aix-Marseille Université and grants from the Agence Nationale de la Recherche (ANR-10-JCJC-1303-03, ANR-14-CE14-0006-02). Work in C.C. laboratory is supported by the CNRS, the Aix-Marseille Université and by grants from the Marseille-Nice Genopole, IBiSA and the Fondation de la Recherche Médicale (FRM DEQ2011-0421282). Ph.D studies of N.F., T.T.H.L. and V.S.N.

are supported by the ANR-14-CE14-0006-02 grant, a fellowship from the University of Sciences and Techniques of Hanoi (USTH) and a fellowship from the French Embassy in Vietnam respectively. M.S.A. was supported by a Ph.D fellowship from the French Ministry of Research.

References

Alcoforado Diniz, J., and Coulthurst, S.J. (2015) Intraspecies competition in *Serratia marcescens* is mediated by Type VI-secreted Rhs effectors and a conserved effector-associated accessory protein. *J Bacteriol* **197**: 2350–2360.

Alcoforado Diniz, J., Liu, Y.C., and Coulthurst, S.J. (2015) Molecular weaponry: diverse effectors delivered by the Type VI secretion system. *Cell Microbiol* **17**:1742–1751.

Aschtgen, M.S., Bernard, C.S., de Bentzmann, S., Lloubes, R., and Cascales, E. (2008) SciN is an outer membrane lipoprotein required for type VI secretion in enteroaggregative *Escherichia coli*. *J. Bacteriol* **190**: 7523–7531.

Aschtgen, M.S., Gavioli, M., Dessen, A., Lloubes, R., and Cascales, E. (2010) The SciZ protein anchors the enteroaggregative *Escherichia coli* Type VI secretion system to the cell wall. *Mol Microbiol* **75**: 886–899.

Ballister, E.R., Lai, A.H., Zuckermann, R.N., Cheng, Y., and Mougous, J.D. (2008) In vitro self-assembly of tailorable nanotubes from a simple protein building block. *Proc Natl Acad Sci USA* **105**: 3733–3738.

Basler, M. (2015) Type VI secretion system: secretion by a contractile nanomachine. *Philos Trans R Soc Lond B Biol Sci* **370**: 20150021.

Basler, M., Pilhofer, M., Henderson, G.P., Jensen, G.J., and Mekalanos, J.J. (2012) Type VI secretion requires a dynamic contractile phage tail-like structure. *Nature* **483**: 182–186.

Battesti, A., and Bouveret, E. (2012) The bacterial two-hybrid system based on adenylate cyclase reconstitution in *Escherichia coli*. *Methods* **58**: 325–334.

Benz, J., and Meinhart, A. (2014) Antibacterial effector/immunity systems: it's just the tip of the iceberg. *Curr Opin Microbiol* **17**: 1–10.

Bonemann, G., Pietrosiuk, A., Diemand, A., Zentgraf, H., and Mogk, A. (2009) Remodelling of VipA/VipB tubules by ClpV-mediated threading is crucial for type VI protein secretion. *EMBO J* **28**: 315–325.

Bonemann, G., Pietrosiuk, A., and Mogk, A. (2010) Tubules and donuts: a type VI secretion story. *Mol Microbiol* **76**: 815–821.

Boyer, F., Fichant, G., Berthod, J., Vandenbrouck, Y., and Attree, I. (2009) Dissecting the bacterial type VI secretion system by a genome wide in silico analysis: what can be learned from available microbial genomic resources? *BMC Genomics* **10**: 104.

Brunet, Y.R., Bernard, C.S., Gavioli, M., Lloubes, R., and Cascales, E. (2011) An epigenetic switch involving overlapping fur and DNA methylation optimizes expression of a type VI secretion gene cluster. *PLoS Genet* **7**: e1002205.

Brunet, Y.R., Espinosa, L., Harchouni, S., Mignot, T., and Cascales, E. (2013) Imaging type VI secretion-mediated bacterial killing. *Cell Rep* **3**: 36–41.

Brunet, Y.R., Henin, J., Celia, H., and Cascales, E. (2014) Type VI secretion and bacteriophage tail tubes share a common assembly pathway. *EMBO Rep* **15**: 315–321.

Brunet, Y.R., Zoued, A., Boyer, F., Douzi, B., and Cascales, E. (2015) The Type VI secretion TssEFGK-VgrG phage-like baseplate is recruited to the TssJLM membrane complex via multiple contacts and serves as assembly platform for tail tube/sheath polymerization. *PLoS Genet* **11**: e1005545.

Carruthers, M.D., Nicholson, P.A., Tracy, E.N., and Munson, R.S., Jr. (2013) Acinetobacter baumannii utilizes a type VI secretion system for bacterial competition. *PLoS One* **8**: e59388.

Cascales, E. (2008) The type VI secretion toolkit. *EMBO Rep* **9**: 735–741.

Coulthurst, S.J. (2013) The Type VI secretion system – a widespread and versatile cell targeting system. *Res Microbiol* **164**: 640–654.

Darrow, A.L., Olson, M.W., Xin, H., Burke, S.L., Smith, C., Schalk-Hihi, C., *et al*. (2011) A novel fluorogenic substrate for the measurement of endothelial lipase activity. *J Lipid Res* **52**: 374–382.

Datsenko, K.A., and Wanner, B.L. (2000) One-step inactivation of chromosomal genes in *Escherichia coli* K-12 using PCR products. *Proc Natl Acad Sci USA* **97**: 6640–6645.

Dereeper, A., Guignon, V., Blanc, G., Audic, S., Buffet, S., Chevenet, F., *et al*. (2008) Phylogeny.fr: robust phylogenetic analysis for the non-specialist. *Nucleic Acids Res* **36**: W465–469.

Ding, J., Wang, W., Feng, H., Zhang, Y., and Wang, D.C. (2012) Structural insights into the *Pseudomonas aeruginosa* type VI virulence effector Tse1 bacteriolysis and self-protection mechanisms. *J Biol Chem* **287**: 26911–26920

Dong, T.G., Ho, B.T., Yoder-Himes, D.R., and Mekalanos, J.J. (2013) Identification of T6SS-dependent effector and immunity proteins by Tn-seq in *Vibrio cholerae*. *Proc Natl Acad Sci USA* **110**: 2623–2628.

Douzi, B., Spinelli, S., Blangy, S., Roussel, A., Durand, E., Brunet, Y.R., *et al*. (2014) Crystal structure and self-interaction of the type VI secretion tail-tube protein from enteroaggregative *Escherichia coli*. *PLoS One* **9**: e86918.

Durand, E., Cambillau, C., Cascales, E., and Journet, L. (2014) VgrG, Tae, Tle, and beyond: the versatile arsenal of Type VI secretion effectors. *Trends Microbiol* **22**: 498–507.

Durand, E., Derrez, E., Audoly, G., Spinelli, S., Ortiz-Lombardia, M., Raoult, D., *et al*. (2012) Crystal structure of the VgrG1 actin cross-linking domain of the *Vibrio cholerae* type VI secretion system. *J Biol Chem* **287**: 38190–38199.

Durand, E., Nguyen, V.S., Zoued, A., Logger, L., Péhau-Arnaudet, G., Aschtgen, M.S, *et al*. (2015) Biogenesis and structure of a type VI secretion membrane core complex. *Nature* **523**: 555–60.

Egan, F., Reen, F.J., and O'Gara, F. (2015) Tle distribution and diversity in metagenomic datasets reveal niche specialization. *Environ Microbiol Rep* **7**: 194–203.

Emsley, P., Lohkamp, B., Scott, W.G., and Cowtan, K. (2010) Features and development of Coot. *Acta Crystallogr D Biol Crystallogr* **66**: 486–501.

van den Ent, F., and Lowe, J. (2006) RF cloning: a restriction-free method for inserting target genes into plasmids. *J Biochem Biophys Methods* **67**: 67–74.

Farber, S.A., Pack, M., Ho, S.Y., Johnson, I.D., Wagner, D.S., Dosch, R., *et al*. (2001) Genetic analysis of digestive physiology using fluorescent phospholipid reporters. *Science* **292**: 1385–1388.

Finn, R.D., Clements, J., Eddy, S.R. (2011) HMMER web server: interactive sequence similarity searching. *Nucl Acids Res* **39**: W29–37.

de la Fournière, L., Ivanova, M.G., Blond, J.-P., Carrière, F., Verger, R. (1994) Surface behaviour of human pancreatic and gastric lipases. *Colloids Surf B* **2**: 585–593.

Gueguen, E., and Cascales, E. (2013) Promoter swapping unveils the role of the *Citrobacter rodentium* CTS1 type VI secretion system in interbacterial competition. *Appl Environ Microbiol* **79**: 32–38.

Hachani, A., Allsopp, L.P., Oduko, Y., and Filloux, A. (2014) The VgrG proteins are "a la carte" delivery systems for bacterial type VI effectors. *J Biol Chem* **289**: 17872–17884.

Ho, B.T., Dong, T.G., and Mekalanos, J.J. (2014) A view to a kill: the bacterial type VI secretion system. *Cell Host Microbe* **15**: 9–21.

Hood, R.D., Singh, P., Hsu, F., Guvener, T., Carl, M.A., Trinidad, R.R., *et al*. (2010) A type VI secretion system of *Pseudomonas aeruginosa* targets a toxin to bacteria. *Cell Host Microbe* **7**: 25–37.

Hu, H., Zhang, H., Gao, Z., Wang, D., Liu, G., Xu, J., *et al*. (2014) Structure of the type VI secretion phospholipase effector Tle1 provides insight into its hydrolysis and membrane targeting. *Acta Crystallogr D Biol Crystallogr* **70**: 2175–2185.

Hullmann, J., Patzer, S.I., Romer, C., Hantke, K., and Braun, V. (2008) Periplasmic chaperone FkpA is essential for imported colicin M toxicity. *Mol Microbiol* **69**: 926–937.

Jiang, F., Waterfield, N.R., Yang, J., Yang, G., and Jin, Q. (2014) A *Pseudomonas aeruginosa* type VI secretion phospholipase D effector targets both prokaryotic and eukaryotic cells. *Cell Host Microbe* **15**: 600–610.

Journet, L., and Cascales, E. (2016) The Type VI secretion system in *Escherichia coli* and related species. *EcoSal-Plus* doi:10.1128/ecosalplus.ESP-0009-2015.

Kapitein, N., Bonemann, G., Pietrosiuk, A., Seyffer, F., Hausser, I., Locker, J.K., and Mogk, A. (2013) ClpV recycles VipA/VipB tubules and prevents non-productive tubule formation to ensure efficient type VI protein secretion. *Mol Microbiol* **87**: 1013–1028.

Karimova, G., Pidoux, J., Ullmann, A., and Ladant, D. (1998) A bacterial two-hybrid system based on a reconstituted signal transduction pathway. *Proc Natl Acad Sci USA* **95**: 5752–5756.

Kelley, L.A., and Sternberg, M.J. (2009) Protein structure prediction on the Web: a case study using the Phyre server. *Nat Protoc* **4**: 363–371.

Kudryashev, M., Wang, R.Y., Brackmann, M., Scherer, S., Maier, T., Baker, D., *et al*. (2015) Structure of the type VI secretion system contractile sheath. *Cell* **160**: 952–62.

Leiman, P.G., Basler, M., Ramagopal, U.A., Bonanno, J.B., Sauder, J.M., Pukatzki, S., *et al*. (2009) Type VI secretion apparatus and phage tail-associated protein complexes share a common evolutionary origin. *Proc Natl Acad Sci USA* **106**: 4154–4159.

Lery, L.M., Frangeul, L., Tomas, A., Passet, V., Almeida, A.S., Bialek-Davenet, S., *et al*. (2014) Comparative analysis of *Klebsiella pneumoniae* genomes identifies a phospholipase D family protein as a novel virulence factor. *BMC Biol* **12**: 41.

Liang, X., Moore, R., Wilton, M., Wong, M.J., Lam, L., and Dong, T.G. (2015) Identification of divergent type VI secretion effectors using a conserved chaperone domain. *Proc Natl Acad Sci USA* **112**: 9106–9111.

Lu, D., Zheng, Y., Liao, N., Wei, L., Xu, B., Liu, X., and Liu, J. (2014) The structural basis of the Tle4-Tli4 complex reveals the self-protection mechanism of H2-T6SS in *Pseudomonas aeruginosa*. *Acta Crystallogr D Biol Crystallogr* **70**: 3233–3243.

Ma, J., Bao, Y., Sun, M., Dong, W., Pan, Z., Zhang, W., Lu, C. and Yao, H. (2014) Two functional type VI secretion systems in avian pathogenic *Escherichia coli* are involved in different pathogenic pathways. *Infect Immun* **82**: 3867–3879

MacIntyre, D.L., Miyata, S.T., Kitaoka, M., and Pukatzki, S. (2010) The *Vibrio cholerae* type VI secretion system displays antimicrobial properties. *Proc Natl Acad Sci USA* **107**: 19520–19524.

Mougous, J.D., Cuff, M.E., Raunser, S., Shen, A., Zhou, M., Gifford, C.A., *et al*. (2006) A virulence locus of *Pseudomonas aeruginosa* encodes a protein secretion apparatus. *Science* **312**: 1526–1530.

Murdoch, S.L., Trunk, K., English, G., Fritsch, M.J., Pourkarimi, E., and Coulthurst, S.J. (2011) The opportunistic pathogen *Serratia marcescens* utilizes type VI secretion to target bacterial competitors. *J Bacteriol* **193**: 6057–6069.

Pell, L.G., Kanelis, V., Donaldson, L.W., Howell, P.L., and Davidson, A.R. (2009) The phage lambda major tail protein structure reveals a common evolution for long-tailed phages and the type VI bacterial secretion system. *Proc Natl Acad Sci USA* **106**: 4160–4165.

Point, V., Benarouche, A., Jemel, I., Parsiegla, G., Lambeau, G., Carriere, F., and Cavalier, J.F. (2013) Effects of the propeptide of group X secreted phospholipase A(2) on substrate specificity and interfacial activity on phospholipid monolayers. *Biochimie* **95**: 51–58.

Pukatzki, S., Ma, A.T., Revel, A.T., Sturtevant, D., and Mekalanos, J.J. (2007) Type VI secretion system translocates a phage tail spike-like protein into target cells where it cross-links actin. *Proc Natl Acad Sci USA* **104**: 15508–15513.

Pukatzki, S., Ma, A.T., Sturtevant, D., Krastins, B., Sarracino, D., Nelson, W.C., *et al*. (2006) Identification of a conserved bacterial protein secretion system in *Vibrio cholerae* using the Dictyostelium host model system. *Proc Natl Acad Sci USA* **103**: 1528–1533.

Russell, A.B., LeRoux, M., Hathazi, K., Agnello, D.M., Ishikawa, T., Wiggins, P.A., *et al*. (2013) Diverse type VI secretion phospholipases are functionally plastic antibacterial effectors. *Nature* **496**: 508–512.

Russell, A.B., Peterson, S.B., and Mougous, J.D. (2014) Type VI secretion system effectors: poisons with a purpose. *Nat Rev Microbiol* **12**: 137–148.

Schwarz, S., West, T.E., Boyer, F., Chiang, W.C., Carl, M.A., Hood, R.D., *et al.* (2010) Burkholderia type VI secretion systems have distinct roles in eukaryotic and bacterial cell interactions. *PLoS Pathog* **6**: e1001068.

Sciara, G., Blangy, S., Siponen, M., Mc Grath, S., van Sinderen, D., Tegoni, M., *et al.* (2008) A topological model of the baseplate of lactococcal phage Tuc2009. *J Biol Chem* **283**: 2716–2723.

Shang, G., Liu, X., Lu, D., Zhang, J., Li, N., Zhu, C. *et al.* (2012) Structural insight into how *Pseudomonas aeruginosa* peptidoglycan hydrolase Tse1 and its immunity protein Tsi1 function. *Biochem J* **448**: 201–211

Shneider, M.M., Buth, S.A., Ho, B.T., Basler, M., Mekalanos, J.J., and Leiman, P.G. (2013) PAAR-repeat proteins sharpen and diversify the type VI secretion system spike. *Nature* **500**: 350–353.

Silverman, J.M., Agnello, D.M., Zheng, H., Andrews, B.T., Li, M., Catalano, C.E., *et al.* (2013) Haemolysin coregulated protein is an exported receptor and chaperone of type VI secretion substrates. *Mol Cell* **51**: 584–593.

Silverman, J.M., Brunet, Y.R., Cascales, E., and Mougous, J.D. (2012) Structure and regulation of the type VI secretion system. *Annu Rev Microbiol* **66**: 453–472.

Spencer, C., and Brown, H.A. (2015) Biochemical characterization of a *Pseudomonas aeruginosa* phospholipase D. *Biochemistry* **54**: 1208–1218.

Spinola-Amilibia, M., Davo-Siguero, I., Ruiz, F.M., Santillana, E., Medrano, F.J., and Romero, A. (2016) The structure of VgrG1 from *Pseudomonas aeruginosa*, the needle tip of the Type VI secretion system. *Acta Cryst. D* **72**: 22–33.

Suarez, G., Sierra, J.C., Erova, T.E., Sha, J., Horneman, A.J., and Chopra, A.K. (2010) A type VI secretion system effector protein, VgrG1, from *Aeromonas hydrophila* that induces host cell toxicity by ADP ribosylation of actin. *J Bacteriol* **192**: 155–168.

Uchida, K., Leiman, P.G., Arisaka, F., and Kanamaru, S. (2014) Structure and properties of the C-terminal beta-helical domain of VgrG protein from *Escherichia coli* O157. *J Biochem* **155**: 173–182.

Unterweger, D., Kostiuk, B., Ötjengerdes, R., Wilton, A., Diaz-Satizabal, L. and Pukatzki, S. (2015) Chimeric adaptor proteins translocate diverse type VI secretion system effectors in *Vibrio cholerae*. *EMBO J* **34**: 2198–2210.

Verger, R., and de Haas, G.H. (1973) Enzyme reactions in a membrane model. 1: a new technique to study enzyme reactions in monolayers. *Chem Phys Lipids* **10**: 127–136.

Whitney, J.C., Beck, C.M., Goo, Y.A., Russell, A.B., Harding, B.N., De Leon, J.A., *et al.* (2014) Genetically distinct pathways guide effector export through the type VI secretion system. *Mol Microbiol* **92**: 529–542.

Whitney, J.C, Quentin, D., Sawai, S., LeRoux, M, Harding, B.N, Ledvina, H.E. *et al.* (2015) An interbacterial NAD(P)(+) glycohydrolase toxin requires elongation factor Tu for delivery to target cells. *Cell* **163**: 607–619.

Zaslaver, A., Bren, A., Ronen, M., Itzkovitz, S., Kikoin, I., Shavit, S., *et al.* (2006) A comprehensive library of fluorescent transcriptional reporters for *Escherichia coli*. *Nat Methods* **3**: 623–628.

Zoued, A., Brunet, Y.R., Durand, E., Aschtgen, M.S., Logger, L., Douzi, B., *et al.* (2014) Architecture and assembly of the Type VI secretion system. *Biochim Biophys Acta* **1843**: 1664–1673.

Zuckert, W.R. (2014) Secretion of bacterial lipoproteins: through the cytoplasmic membrane, the periplasm and beyond. *Biochim Biophys Acta* **1843**: 1509–1516.

Supporting information

Additional supporting information may be found in the online version of this article at the publisher's web-site.